The most specific characteristic of dystrophic muscles is their particular sensitivity to eccentric (lengthening) contractions [26]. Indeed, repeated eccentric work of dystrophic muscles has been shown to induce a large and progressive loss of force as well as an important increase of membrane permeability which can be detected by the release of creatine kinase or by the uptake of membrane-impermeable dyes such as procion orange and Evans Blue dye. It is generally accepted that this is due to an abnormal fragility of the membrane, given the lack of connection between the cytoskeleton and the extracellular matrix. We tested an alternative hypothesis according to which muscle sensitivity to stretch would be primarily due to the abnormal presence at the plasma membrane or to the abnormal regulation of TRPV2 channels. We therefore studied eccentric contractions of EDL muscles from *mdx* mice expressing or not the dominant negative mutant of TRPV2. The progressive loss of force developed by muscles of these mice was very much reduced in comparison to *mdx* control mice, suggesting the involvement of TRPV2 channel in the increased sensitivity of dystrophic muscle to eccentric contractions. Interestingly, the uptake of procion orange dye was also significantly reduced, suggesting that the entry of Ca^{2+} through TRPV2 precedes the large increase of non-specific membrane permeability.

2. Materials and methods

2.1. Animals

Dystrophin-deficient C57BL/10ScSn-*DMD*^{mdx} (*mdx*) mice and their control C57 were from Jackson Laboratories. Generation of TRPV2 dominant negative (TRPV2-DN) transgenic mice (expressing the hemagglutinin (HA)-tagged E604 K mutant TRPV2 channel under the control of the α-skeletal actin promoter in skeletal muscle) has been described previously [22]. Male homozygous TRPV2-DN mice were mated with female *mdx* mice and the resulting male *mdx*/TRPV2-DN were analyzed.

All mice analyzed were 12–16 weeks of age. The experiments were approved by the Animal Ethics Committee of the Catholic University of Louvain, Brussels.

2.2. Muscle mechanical protocol

Mice were deeply anesthetized by intraperitoneal injection of a solution containing ketamine (10 mg ml^{-1}) and xylazine (1 mg ml^{-1}) in order to preserve muscle perfusion during dissection of extensor digitorum longus (EDL) and tibialis anterior muscles. Depth of anesthesia was assessed by the abolition of eyelid and pedal reflexes. After dissection, the animals were killed by cervical dislocation.

EDL muscles were bathed in a 1 ml horizontal chamber continuously superfused with HEPES buffered Krebs solution (100% O_2) containing (in mM): NaCl 135.5, KCl 5.9, $MgCl_2$ 1.2, $CaCl_2$ 2.5, HEPES sodium 11.6 and glucose 11.5, and maintained at a temperature of 20 ± 0.1 °C. One end of the muscle was tied to an isometric force transducer, and the other to an electromagnetic motor and length transducer. Stimulation (125 Hz) was delivered through platinum electrodes running in parallel to the muscles. Optimum muscle length (L_0) was carefully adjusted for maximal isometric force using 300 ms maximally fused tetani. Force was digitalized at a sampling rate of 1 kHz, using a PCI 6023E i/o card (National Instruments). Normalized stress was expressed relative to cross-sectional area, obtained by multiplying absolute force by the quotient "muscle fiber length (mm)/muscle blotted weight (mg)" and considering the fiber length equal to 0.5 × L_0 for EDL [27].

The muscles were subjected to a series of seven eccentric contractions consisting in 500 ms tetani during which a stretch of 1 mm (L_0 to L_0 + 8%) at a speed of 1 L_0 s^{-1} was applied 160 ms after the start of stimulation and maintained up to 250 ms after the start of stimulation (10 s interval between two successive tetani). Isometric force was measured for each tetanus just before the onset of the stretch and the percentage force drop was calculated.

2.3. Assessment of sarcolemmal damage

The stimulated muscle and its non-stimulated contralateral control were both bathed for 1 h in the oxygenated Krebs solution containing 1% procion orange. This dye is known to be excluded from intact cells but to penetrates damaged membranes [26,28]. The muscles were then rinsed twice in normal Krebs solution and were finally rapidly frozen in isopentane precooled with liquid N_2. Transverse 10 μm thick sections were cut from muscle midbelly region, mounted with vectashield solution and viewed in epifluorescence (Zeiss S100 inverted microscope, FITC filters). The area of procion orange positive fibers was measured as a percentage of the entire muscle cross-sectional area using ImageJ program (NCBI).

2.4. Reagents

The GsMTx4 toxin, isolated from *Grammostola spatulata* spider [29], was obtained from PeptaNova (Sandhausen, Germany); SFK-96365 (1-[B-[3-(4-methoxyphenyl)propoxy]-4-methoxyphenethyl]-1H-imidazole) from Alexis Corporation (Lausen, Switzerland)

2.5. Statistical analysis

Data are presented as means ± S.E.M. Unpaired *t*-tests were used to compare two groups and ANOVA to compare many groups. Significance level was fixed at $P < 0.05$.

3. Results

3.1. Dominant-negative inhibition of endogenous TRPV2 reduces the sensitivity of dystrophic muscle (mdx) to eccentric contractions

Isolated EDL muscles from *mdx* mice were submitted to successive eccentric contractions. We observed that dystrophin-deficient muscles presented a specific and progressive force drop (Fig. 1A and B). After six lengthening contractions, *mdx* muscles were able to develop less than 10% of the initial force; in the same conditions, their controls (C57) still developed 80% of the initial force. We and others previously reported that the channels abnormally activated in *mdx* fibers were sensitive to store depletion and membrane stretch [11,30,32]. In particular, we showed that they were sensitive to SKF-96365, a non-specific inhibitor of TRP channels [33] and to GsMTx4 toxin, the most specific inhibitor of mechanosensitive channels known today [29]. We therefore investigated the effect of these compounds on the sensitivity of *mdx* muscles to eccentric contractions. We observed that muscles incubated in the presence of 30 μM SKF-96365 (10 min preincubation) or in the presence of 10 μM GsMTx4 (2 h preincubation) developed significantly more force after a series of lengthening contractions than in the absence of the inhibitors (data not shown). These results confirm data reported by other groups using different eccentric contractions protocols [34] and suggest the involvement of these channels in the sensitivity to eccentric contractions. Since the best candidate of stretch-activated channel in skeletal muscle is TRPV2 [25], we studied the process on EDL muscles from normal C57 and dystrophic *mdx* mice expressing or not a dominant-negative mutant of TRPV2 (TRPV2-DN) [22]. We first observed that EDL muscles from *mdx* mice were bigger but developed less isometric

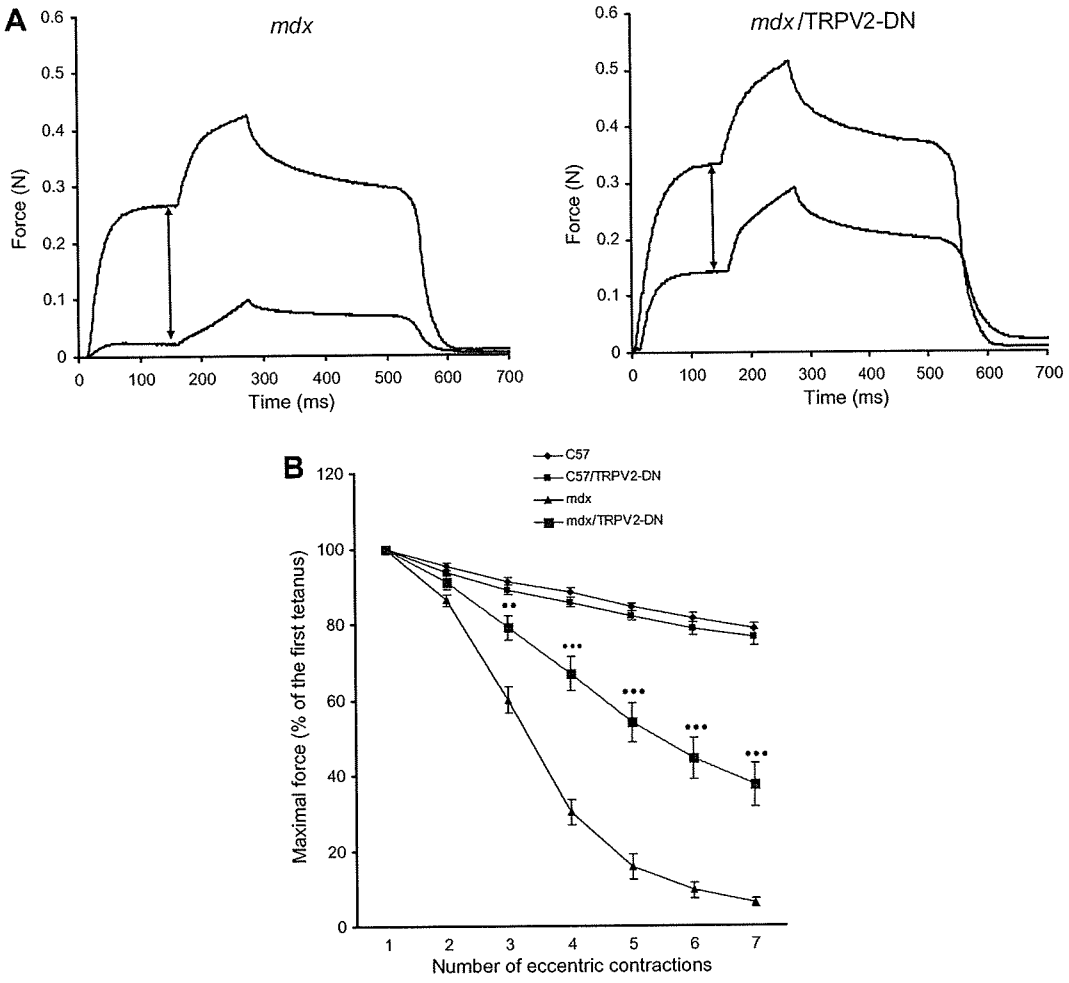

Fig. 1. Sensitivity to eccentric contractions. (A) Force traces of EDL muscle from *mdx* (left panel) and *mdx*/TRPV2-DN (right panel) mice. First and seventh tetanus presented. (B) Quantification of the force produced during repetitive eccentric contractions of EDL muscles from C57, C57/TRPV2, *mdx* and *mdx*/TRPV2. $^{**}P < 0.01$; $^{***}P < 0.001$ (one way repeated measures ANOVA, $n = 5–8$).

Table 1
Mechanicals properties of EDL muscles.

	C57	C57/TRPV2-DN	*mdx*	*mdx*/TRPV2-DN
Muscle weight (mg)	10.11 ± 0.22	9.84 ± 0.17	13.99 ± 0.49[a]	12.48 ± 0.31[a,b]
L_0 (mm)	11.75 ± 0.17	11.96 ± 0.26	11.82 ± 0.09	11.95 ± 0.09
F_0 (mN)	327.50 ± 32.88	358.46 ± 22.01	345.71 ± 21.87	330.73 ± 15.28
S_0 (mN/mm^2)	188.88 ± 16.93	219.23 ± 16.53	147.14 ± 9.85[a]	157.95 ± 3.98
n	5	8	8	6

[a] $P < 0.05$ vs C57.
[b] $P < 0.05$ vs *mdx*.

tension than controls (Table 1; Two way ANOVA, $P < 0.05$). This muscle pseudohypertrophy has been previously described in *mdx* mice [35]. Interestingly, in *mdx*/TRPV2-DN mice, EDL pseudohypertrophy was reduced (muscle weight significantly lower in *mdx*/TRPV2-DN than in *mdx*, and isometric tension slightly but not significantly higher in *mdx*/TRPV2-DN than in *mdx*, Table 1). When submitted to a series of eccentric contractions, EDL muscles from *mdx*/TRPV2-DN presented a much lower force drop than EDL from *mdx* mice (Fig. 1, one way repeated measures ANOVA, $P < 0.01–0.001$). The expression of TRPV2-DN had no effect on the force developed by C57 muscles during lengthening contractions.

These results strongly suggest a major role of TRPV2 channel in the stretch-induced force drop observed in *mdx* muscles.

3.3. Effect of dominant-negative inhibition of TRPV2 on stretch-induced membrane permeability in isolated muscles

To test whether the force drop in *mdx* muscle was correlated with the membrane permeability, isolated muscles were incubated for 1 h after a series of eccentric contractions in oxygenated Krebs solution containing 1% procion orange (a fluorescent dye substance which is excluded from intact cells but penetrate cells with membrane damage). Muscle cross-sections were analyzed for the percentage of procion orange positive fibers area related to the global area of the muscle section. As illustrated in Fig. 2, *mdx* muscles expressing the dominant negative mutant of TRPV2 presented a large reduction of the procion orange positive area compared to

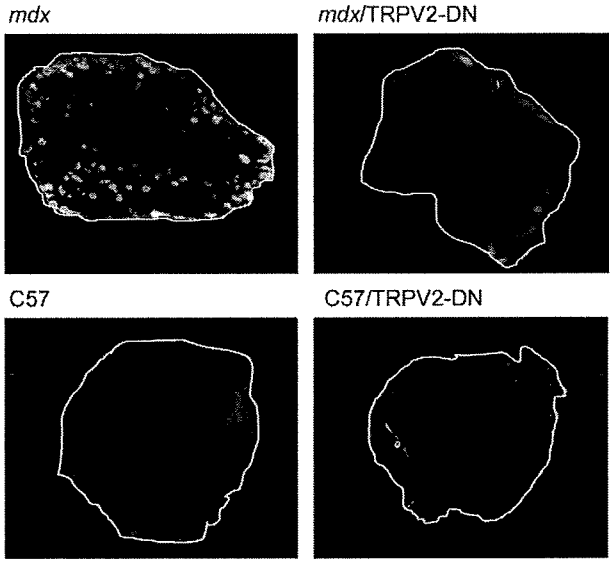

Fig. 2. Permeability to procion orange dye. Transverse sections of EDL muscles submitted to a series of seven lengthening contractions and then immersed during 1 h in procion orange containing Krebs solution. Sections examined under FITC fluorescence microscopy.

their *mdx* controls (11.46 ± 1.01% in *mdx*/TRPV2-DN vs 29.00 ± 3.72% in *mdx*, $n = 3$, $P < 0.05$). We checked that C57 and C57/TRPV2-DN muscles submitted to a series of eccentric contractions had a procion orange positive area that was always very low (below 5% of the total area) and limited to the periphery of muscles. Similarly, unstretched muscles (from C57, C57/TRPV2-DN, *mdx* and *mdx*/TRPV2-DN mouse strains) also present a negligible basal level of procion orange positive area.

4. Discussion

Since a long time, the importance of an abnormal influx of Ca^{2+} has been studied in skeletal myotubes from DMD patients [36] and in myotubes and adult fibers from *mdx* mice [14,37–40]. This influx has been shown to implicate various spontaneously active, store-dependent and/or mechanosensitive cationic channels [36,41] whereas the voltage-dependent Ca channels did not seem to be involved [41]. Accordingly, the channels involved were inhibited by lanthanides (Gd^{3+}, La^{3+}) and by pharmacological agents such as SKF-96365 and GsMTx4 toxin. We and others also showed that their occurrence at the membrane increased after myocyte stretch and after stimulation with IGF-1 [25,31,42], suggesting that they could be constituted of TRPV2 proteins [25,43,44]. This was clearly demonstrated recently. Indeed, transgenic or adenoviral expression of a dominant-negative TRPV2 in *mdx* muscles reduced several indices of the severity of the disease such as elevated serum creatine kinase level, number of apoptotic and necrotic fibers, intensity of the regeneration (central nuclei) and the consecutive fibrosis [22].

In the present study, we investigated the possible involvement of TRPV2 ion channel in the sensitivity of dystrophic muscle of *mdx* mice to eccentric contraction. This sensitivity constitutes the characteristic feature of the disease: forced lengthenings produce an important loss of force in dystrophic muscles [26,45]. This property is clearly related to membrane permeability and does not arise from factors within myofibrils [46]. Muscle fiber lesions resulting from eccentric contractions can be visualized by penetration of membrane-impermeant dyes like orange procion, suggesting that stretch of dystrophin-deficient membrane induces membrane tears, at least transiently [28]. Interestingly a linear relationship was observed between the percentage of orange procion positive fibers and the peak of tension observed at the end of eccentric contraction [45] and the force drop [47], suggesting that the high strain imposed on the fiber during forced lengthening produces localized disruptions of the plasma membrane that impairs mechanical response to electrical stimulation. However, the percentage of orange procion positive fibers was always smaller than the force drop (slope of relationship < 1). This was attributed to the fact that membrane lesions are localized; a single localized lesion completely prevents fiber contraction but as diffusion of the dyes is restricted, histochemical detection of these lesions could be under-estimated (few sections analyzed in a complete muscle) [2]. In this view, the increased fragility of the membrane due to the absence of dystrophin would explain the sensitivity of *mdx* muscles to eccentric contraction. However, this explanation was challenged by the observation that in muscles strained up to the point of membrane rupture, the absence of dystrophin had no detectable effect on the stress, the strain, or the energy absorbed, regardless of the state of muscle activation [48]. An alternative explanation was proposed by the group of Allen, who showed that short-term damage of *mdx* muscle fibers caused by stretch was partially prevented by blocking mechanosensitive channels [34,49]. This was confirmed here on isolated EDL muscles with a much milder protocol (8% stretch at $1\ L_0\ s^{-1}$ in our experiments vs 40% stretch at $4\ L_0\ s^{-1}$ in [49]). Interestingly, eccentric contractions also allowed an entry of Na^+ in *mdx* fibers through the same stretch-activated channels [50]. The prolonged increase of intracellular Na^+ concentration consecutive to eccentric contractions suggests that the loss of tension might be due, at least partially, not only to membrane damage but also to a prolonged membrane depolarization. This would explain the discrepancy between the percentage of damaged fibers (permeabilized to orange procion) and the amplitude of the force drop (see above). Here we compared the sensitivity to eccentric contractions in muscles from dystrophic mice expressing or not a dominant-negative TRPV2 channel. We show that muscles expressing the mutated channel are partially protected against eccentric contractions. Not only the force drop was very reduced, but the permeability to procion orange dye was significantly decreased, suggesting that the entry of ions through these channels precedes and is implicated in membrane lesions. This is in agreement with a recent study showing that reducing extracellular Ca^{2+} concentration or inhibiting calpain activity with leupeptin during lengthening contractions not only improved the force maintained but minimized membrane disruption [51]. This does not rule out an involvement of membrane fragility. Indeed, a significant force drop consecutive to repeated eccentric contractions is nevertheless still observed in dystrophic muscles expressing the dominant-negative TRPV2 mutant. Alternatively, this might be due to the fact that the entry of Ca^{2+} through native TRPV2 channels is not completely abolished in these muscles [22].

In conclusion, this study identifies TRPV2 as the mechanosensitive channel involved in eccentric work-induced force drop observed in dystrophic muscles. It suggests that the entry of cations, among which Ca^{2+}, through this channel is, at least partially, responsible for the observed membrane disruptions. Therefore, it constitutes a potentially interesting pharmacological target for the treatment of Duchenne muscular dystrophy.

Acknowledgements

We warmly thank M.L. Cao and M. Van Schoor for excellent technical assistance. We also acknowledge Dr. N. Tajeddine for helpful discussions. This work was supported by the "Association française contre les myopathies" (AFM), the "Association belge contre les maladies neuro-musculaires" (ABMM) and by a Grant

ARC 05/10-328 from the General Direction of Scientific Research of the French Community of Belgium.

References

[1] Blake, D.J., Weir, A., Newey, S.E. and Davies, K.E. (2002) Function and genetics of dystrophin and dystrophin-related proteins in muscle. Physiol. Rev. 82, 291–329.

[2] Gillis, J.M. (1999) Understanding dystrophinopathies: an inventory of the structural and functional consequences of the absence of dystrophin in muscles of the *mdx* mouse. J. Muscle Res. Cell Motil. 20, 605–625.

[3] Monaco, A.P., Neve, R.L., Colletti-Feener, C., Bertelson, C.J., Kurnit, D.M. and Kunkel, L.M. (1986) Isolation of candidate cDNAs for portions of the Duchenne muscular dystrophy gene. Nature 323, 646–650.

[4] Hoffman, E.P., Brown Jr., R.H. and Kunkel, L.M. (1987) Dystrophin: the protein product of the Duchenne muscular dystrophy locus. Cell 51, 919–928.

[5] Ervasti, J.M. and Campbell, K.P. (1991) Membrane organization of the dystrophin–glycoprotein complex. Cell 66, 1121–1131.

[6] Culligan, K.G., Mackey, A.J., Finn, D.M., Maguire, P.B. and Ohlendieck, K. (1998) Role of dystrophin isoforms and associated proteins in muscular dystrophy. Int. J. Mol. Med. 2, 639–648.

[7] Ervasti, J.M. and Campbell, K.P. (1993) A role for the dystrophin–glycoprotein complex as a transmembrane linker between laminin and actin. J. Cell Biol. 122, 809–823.

[8] Carlson, C.G. (1996) Acetylcholine receptor and calcium leakage activity in nondystrophic and dystrophic myotubes (MDX). Muscle Nerve 19, 1258–1267.

[9] Haws, C.M. and Lansman, J.B. (1991) Developmental regulation of mechanosensitive calcium channels in skeletal muscle from normal and *mdx* mice. Proc. Biol. Sci. 245, 173–177.

[10] Franco Jr., A. and Lansman, J.B. (1990) Calcium entry through stretch-inactivated ion channels in *mdx* myotubes. Nature 344, 670–673.

[11] Franco-Obregon Jr., A. and Lansman, J.B. (1994) Mechanosensitive ion channels in skeletal muscle from normal and dystrophic mice. J. Physiol. 481, 299–309.

[12] Ruegg, U.T. and Gillis, J.M. (1999) Calcium homeostasis in dystrophic muscle. Trends Pharmacol. Sci. 20, 351–352.

[13] Gailly, P. (2002) New aspects of calcium signaling in skeletal muscle cells: implications in Duchenne muscular dystrophy. Biochim. Biophys. Acta 1600, 38–44.

[14] Turner, P.R., Westwood, T., Regen, C.M. and Steinhardt, R.A. (1988) Increased protein degradation results from elevated free calcium levels found in muscle from *mdx* mice. Nature 335, 735–738.

[15] Badalamente, M.A. and Stracher, A. (2000) Delay of muscle degeneration and necrosis in *mdx* mice by calpain inhibition. Muscle Nerve 23, 106–111.

[16] Gailly, P., De Backer, F., Van Schoor, M. and Gillis, J.M. (2007) In situ measurements of calpain activity in isolated muscle fibres from normal and dystrophin-lacking *mdx* mice. J. Physiol. 582, 1261–1275.

[17] Iyer, S.L., Katyare, S.S. and Howland, J.L. (1976) Elevated erythrocyte phospholipase A associated with Duchenne and myotonic muscular dystrophy. Neurosci. Lett. 2, 103–106.

[18] Boittin, F.X., Petermann, O., Hirn, C., Mittaud, P., Dorchies, O.M., Roulet, E. and Ruegg, U.T. (2006) Ca^{2+}-independent phospholipase A_2 enhances store-operated Ca^{2+} entry in dystrophic skeletal muscle fibers. J. Cell Sci. 119, 3733–3742.

[19] Vandebrouck, A. et al. (2006) Regulation of store-operated calcium entries and mitochondrial uptake by minidystrophin expression in cultured myotubes. FASEB J. 20, 136–138.

[20] Ragusa, R.J., Chow, C.K. and Porter, J.D. (1997) Oxidative stress as a potential pathogenic mechanism in an animal model of Duchenne muscular dystrophy. Neuromuscul. Disord. 7, 379–386.

[21] Shkryl, V.M., Martins, A.S., Ullrich, N.D., Nowycky, M.C., Niggli, E. and Shirokova, N. (2009) Reciprocal amplification of ROS and Ca^{2+} signals in stressed *mdx* dystrophic skeletal muscle fibers. Pflugers Arch. 458, 915–928.

[22] Iwata, Y., Katanosaka, Y., Arai, Y., Shigekawa, M. and Wakabayashi, S. (2009) Dominant-negative inhibition of Ca^{2+} influx via TRPV2 ameliorates muscular dystrophy in animal models. Hum. Mol. Genet. 18, 824–834.

[23] Damann, N., Voets, T. and Nilius, B. (2008) TRPs in our senses. Curr. Biol. 18, R880–R889.

[24] Muraki, K., Iwata, Y., Katanosaka, Y., Ito, T., Ohya, S., Shigekawa, M. and Imaizumi, Y. (2003) TRPV2 is a component of osmotically sensitive cation channels in murine aortic myocytes. Circ. Res. 93, 829–838.

[25] Iwata, Y., Katanosaka, Y., Arai, Y., Komamura, K., Miyatake, K. and Shigekawa, M. (2003) A novel mechanism of myocyte degeneration involving the Ca^{2+}-permeable growth factor-regulated channel. J. Cell Biol. 161, 957–967.

[26] Moens, P., Baatsen, P.H. and Marechal, G. (1993) Increased susceptibility of EDL muscles from *mdx* mice to damage induced by contractions with stretch. J. Muscle Res. Cell Motil. 14, 446–451.

[27] Brooks, S.V. and Faulkner, J.A. (1988) Contractile properties of skeletal muscles from young, adult and aged mice. J. Physiol. 404, 71–82.

[28] Bansal, D., Miyake, K., Vogel, S.S., Groh, S., Chen, C.C., Williamson, R., McNeil, P.L. and Campbell, K.P. (2003) Defective membrane repair in dysferlin-deficient muscular dystrophy. Nature 423, 168–172.

[29] Suchyna, T.M., Johnson, J.H., Hamer, K., Leykam, J.F., Gage, D.A., Clemo, H.F., Baumgarten, C.M. and Sachs, F. (2000) Identification of a peptide toxin from *Grammostola spatulata* spider venom that blocks cation-selective stretch-activated channels. J. Gen. Physiol. 115, 583–598.

[30] Vandebrouck, C., Martin, D., Colson-Van Schoor, M., Debaix, H. and Gailly, P. (2002) Involvement of TRPC in the abnormal calcium influx observed in dystrophic (*mdx*) mouse skeletal muscle fibers. J. Cell Biol. 158, 1089–1096.

[31] Ducret, T., Vandebrouck, C., Cao, M.L., Lebacq, J. and Gailly, P. (2006) Functional role of store-operated and stretch-activated channels in murine adult skeletal muscle fibres. J. Physiol. 575, 913–924.

[32] Suchyna, T.M. and Sachs, F. (2007) Mechanosensitive channel properties and membrane mechanics in mouse dystrophic myotubes. J. Physiol. 581, 369–387.

[33] Putney, J.W. (2001) The pharmacology of capacitative calcium entry. Mol. Interventions 1, 84–94.

[34] Yeung, E.W., Whitehead, N.P., Suchyna, T.M., Gottlieb, P.A., Sachs, F. and Allen, D.G. (2005) Effects of stretch-activated channel blockers on $[Ca^{2+}]_i$ and muscle damage in the *mdx* mouse. J. Physiol. 562, 367–380.

[35] Lynch, G.S., Hinkle, R.T., Chamberlain, J.S., Brooks, S.V. and Faulkner, J.A. (2001) Force and power output of fast and slow skeletal muscles from mdx mice 6–28 months old. J. Physiol. 535, 591–600.

[36] Imbert, N., Vandebrouck, C., Constantin, B., Duport, G., Guillou, C., Cognard, C. and Raymond, G. (1996) Hypoosmotic shocks induce elevation of resting calcium level in Duchenne muscular dystrophy myotubes contracting in vitro. Neuromuscul. Disord. 6, 351–360.

[37] Tutdibi, O., Brinkmeier, H., Rudel, R. and Fohr, K.J. (1999) Increased calcium entry into dystrophin-deficient muscle fibres of MDX and ADR-MDX mice is reduced by ion channel blockers. J. Physiol. 515 (Pt 3), 859–868.

[38] Mallouk, N. and Allard, B. (2000) Stretch-induced activation of Ca^{2+}-activated K^+ channels in mouse skeletal muscle fibers. Am. J. Physiol. Cell Physiol. 278, C473–C479.

[39] Gailly, P., Boland, B., Himpens, B., Casteels, R. and Gillis, J.M. (1993) Critical evaluation of cytosolic calcium determination in resting muscle fibres from normal and dystrophic (*mdx*) mice. Cell Calcium 14, 473–483.

[40] Gailly, P., Hermans, E., Octave, J.N. and Gillis, J.M. (1993) Specific increase of genetic expression of parvalbumin in fast skeletal muscles of *mdx* mice. FEBS Lett. 326, 272–274.

[41] Imbert, N., Vandebrouck, C., Duport, G., Raymond, G., Hassoni, A.A., Constantin, B., Cullen, M.J. and Cognard, C. (2001) Calcium currents and transients in co-cultured contracting normal and Duchenne muscular dystrophy human myotubes. J. Physiol. 534, 343–355.

[42] Rolland, J.F., De Luca, A., Burdi, R., Andreetta, F., Confalonieri, P. and Conte Camerino, D. (2006) Overactivity of exercise-sensitive cation channels and their impaired modulation by IGF-1 in *mdx* native muscle fibers: beneficial effect of pentoxifylline. Neurobiol. Dis. 24, 466–474.

[43] Kanzaki, M., Zhang, Y.Q., Mashima, H., Li, L., Shibata, H. and Kojima, I. (1999) Translocation of a calcium-permeable cation channel induced by insulin-like growth factor-I. Nat. Cell Biol. 1, 165–170.

[44] Kowase, T., Nakazato, Y., Yoko, O.H., Morikawa, A. and Kojima, I. (2002) Immunohistochemical localization of growth factor-regulated channel (GRC) in human tissues. Endocr. J. 49, 349–355.

[45] Petrof, B.J., Shrager, J.B., Stedman, H.H., Kelly, A.M. and Sweeney, H.L. (1993) Dystrophin protects the sarcolemma from stresses developed during muscle contraction. Proc. Natl. Acad. Sci. USA 90, 3710–3714.

[46] Lynch, G.S., Rafael, J.A., Chamberlain, J.S. and Faulkner, J.A. (2000) Contraction-induced injury to single permeabilized muscle fibers from *mdx*, transgenic *mdx*, and control mice. Am. J. Physiol. Cell Physiol. 279, C1290–C1294.

[47] Deconinck, N., Rafael, J.A., Beckers-Bleukx, G., Kahn, D., Deconinck, A.E., Davies, K.E. and Gillis, J.M. (1998) Consequences of the combined deficiency in dystrophin and utrophin on the mechanical properties and myosin composition of some limb and respiratory muscles of the mouse. Neuromuscul. Disord. 8, 362–370.

[48] Law, D.J., Caputo, A. and Tidball, J.G. (1995) Site and mechanics of failure in normal and dystrophin-deficient skeletal muscle. Muscle Nerve 18, 216–223.

[49] Yeung, E.W., Head, S.I. and Allen, D.G. (2003) Gadolinium reduces short-term stretch-induced muscle damage in isolated *mdx* mouse muscle fibres. J. Physiol. 552, 449–458.

[50] Yeung, E.W., Ballard, H.J., Bourreau, J.P. and Allen, D.G. (2003) Intracellular sodium in mammalian muscle fibers after eccentric contractions. J. Appl. Physiol. 94, 2475–2482.

[51] Zhang, B.T., Yeung, S.S., Allen, D.G., Qin, L. and Yeung, E.W. (2008) Role of the calcium-calpain pathway in cytoskeletal damage after eccentric contractions. J. Appl. Physiol. 105, 352–357.

X-ray Structure Analysis Online 2009, VOL. 25

X-ray Structure Analysis Online

Crystal Structure of Ganciclovir

Tomoko KAWAMURA and Noriaki HIRAYAMA†

Basic Medical Science and Molecular Medicine, Tokai University School of Medicine, 143 Shimokasuya, Isehara, Kanagawa 259-1193, Japan

The crystal of the title compound, $C_9H_{13}N_5O_4$, belongs to space group $P2_1$ with cell dimensions a = 4.380(2), b = 10.909(4), c = 11.601(4)Å, and β = 99.11(3)°. The final R value is 0.0583. The chain moiety corresponding to the ribose ring in guanosine does not adopt a fully extended conformation. The relative orientation of the purine ring and the ether oxygen atom is similar to that observed in one of the crystallographically independent guanosine molecules in the crystal structure of guanosine dehydrate.

(Received December 24, 2008; Accepted February 27, 2009; Published on web May 10, 2009)

Ganciclovir (9-((1,3-dihydroxypropan-2-yloxy)methyl)-2-amino-1*H*-purin-6(9*H*)-one) is an acyclic guanine nucleoside analog, which has inhibitory activity against all herpesviruses, but is especially active against cytomegalovirus (CMV).[1] Ganciclovir inhibits viral DNA synthesis. It is phosphorylated to a deoxyguanosine triphosphate (dGTP) analogue. This competitively inhibits the incorporation of dGTP by viral DNA polymerase, resulting in terminating the elongation of viral DNA. Ganciclovir is effective for the treatment and chronic suppression of CMV rerinitis in immunocompromised patients, and the prevention of CMV disease in transplant patients. Although Ganciclovir is widely used as an antiviral agent, the three-dimensional structure has not been determined so far. An X-ray analysis of the title compound was undertaken to disclose its inherent three-dimensional structure, which is essential for the development of better antiviral drugs.

Ganciclovir was purchased from Sigma. Single crystals of the molecule were grown from a dimethylformamide solution. Despite repeated crystallization, it was extremely difficult to obtain good single crystals. The biggest single crystal after many crystallization experiments was a colorless fine-needle crystal with a size of 0.3 × 0.01 × 0.01 mm. It was mounted on a glass fiber, and used for data collection. The structure was solved by direct methods, and non-H atoms were refined by a full-matrix least-squares method with anisotropic temperature factors. The positions of H-atoms of the amino and hydroxyl groups were obtained from Fourier syntheses. The positions of other H-atoms were geometrically calculated. H-atoms were not refined. An elongated thermal ellipsoid of C8 is indicative of disorder, but it was not possible to separate the disordered positions. The crystal and experimental data are given in Table 1.

The molecular structure, drawn by ORTEP-III,[4] is shown in Fig. 2. Selected bond lengths and bond angles are given in Table 2. The bond lengths and angles are within the expected ranges. The geometrical parameters in the purine ring do not differ significantly from the corresponding values in the guanosine molecules in the crystal structure of guanosine dihydrate.[5] The chain moiety corresponding to the ribose ring in guanosine does not adopt a fully extended conformation with the torsion angles of N4-C6-O2-C7, C6-O2-C7-C9 and O2-C7-

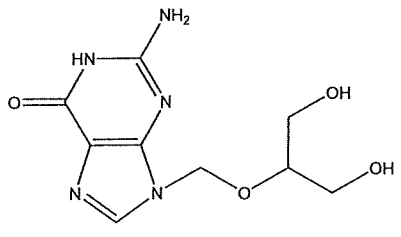

Fig. 1 Chemical structure of ganciclovir..

Table 1 Crystal and experimental data

Formula: $C_9H_{13}N_5O_4$	
Formula weight = 255.23	
Crystal system: monoclinic	
Space group: $P2_1$	$Z = 2$
a = 4.380(2)Å	
b = 10.909(4)Å	β = 99.11(3)°
c = 11.601(4)Å	
V = 547.3(3)Å^3	
D_x = 1.549 g/cm^3	
No. of observations (all) = 1713	
θ_{max} = 68.09° with Cu K_α	
R ($I > 2.00\sigma(I)$) = 0.0583	
Rw(all) = 0.0561	
$(\Delta/\sigma)_{max}$ = 0.005	
$(\Delta\rho)_{max}$ = 0.45 e/Å^3	
$(\Delta\rho)_{min}$ = –0.78 e/Å^3	
Measurement: Rigaku RAXIS-RAPID	
Program system: CrystalStructure 3.6.0[1]	
Structure determination: SIR92[2]	
Refinement: full-matrix	
CCDC deposition number: 714337	

† To whom correspondence should be addressed.
E-mail: hirayama@is.icc.u-tokai.ac.jp

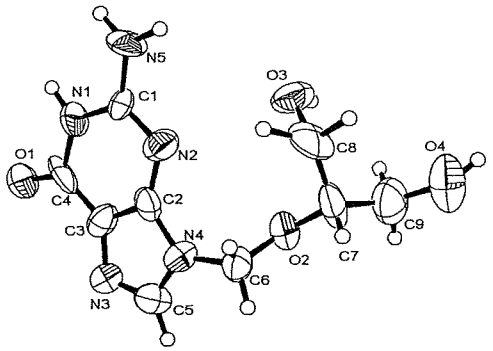

Fig. 2 Molecular structure of ganciclovir along with the labeling atoms. Thermal ellipsoids of non-H atoms are drawn at the 50% probability level.

Table 2 Selected bond lengths (Å), bond angles (°) and torsion angles (°)

O(1)—C(4)	1.25(1)	O(2)—C(6)	1.42(1)
O(2)—C(7)	1.45(1)	O(3)—C(8)	1.33(2)
O(4)—C(9)	1.45(2)	N(1)—C(1)	1.37(1)
N(1)—C(4)	1.38(2)	N(2)—C(1)	1.36(1)
N(2)—C(2)	1.35(2)	N(3)—C(3)	1.38(1)
N(3)—C(5)	1.31(2)	N(4)—C(2)	1.38(1)
N(4)—C(5)	1.36(1)	N(4)—C(6)	1.48(1)
N(5)—C(1)	1.35(1)		
C(7)—O(2)—C(6)	110.1(7)	C(4)—N(1)—C(1)	126.9(9)
C(2)—N(2)—C(1)	111.0(8)	C(5)—N(3)—C(3)	100.5(8)
C(5)—N(4)—C(2)	106.1(8)	C(6)—N(4)—C(2)	124.4(8)
C(6)—N(4)—C(5)	129.5(8)	N(1)—C(1)—N(2)	122.7(9)
N(1)—C(1)—N(5)	118.3(9)	N(2)—C(1)—N(5)	119.0(9)
N(2)—C(2)—N(4)	126.7(8)	N(2)—C(2)—C(3)	130(1)
N(4)—C(2)—C(3)	102.9(9)	N(3)—C(3)—C(2)	114.5(9)
N(3)—C(3)—C(4)	128.1(9)	O(1)—C(4)—N(1)	120(1)
O(1)—C(4)—C(3)	129(1)	N(1)—C(4)—C(3)	111.7(8)
N(3)—C(5)—N(4)	115.9(9)	O(2)—C(6)—N(4)	104.3(7)
O(2)—C(7)—C(8)	109.0(9)	O(2)—C(7)—C(9)	102.5(8)
O(3)—C(8)—C(7)	109(1)	O(4)—C(9)—C(7)	107.4(9)
C(7)—O(2)—C(6)—N(4)	152.7(7)	C(6)—O(2)—C(7)—C(8)	-77(1)
C(6)—O(2)—C(7)—C(9)	155.4(8)	C(4)—N(1)—C(1)—N(2)	-2(2)
C(4)—N(1)—C(1)—N(5)	178(1)	C(1)—N(1)—C(4)—O(1)	178(1)
C(1)—N(1)—C(4)—C(3)	1(2)	C(2)—N(2)—C(1)—N(1)	2(2)
C(2)—N(2)—C(1)—N(5)	-178(1)	C(1)—N(2)—C(2)—N(4)	179(1)
C(1)—N(2)—C(2)—C(3)	-2(2)	C(5)—N(3)—C(3)—C(2)	2(1)
C(5)—N(3)—C(3)—C(4)	179(1)	C(3)—N(3)—C(5)—N(4)	-1(1)
C(5)—N(4)—C(2)—N(2)	-179(1)	C(5)—N(4)—C(2)—C(3)	1(1)
C(6)—N(4)—C(2)—N(2)	2(2)	C(6)—N(4)—C(2)—C(3)	-177.5(9)
C(2)—N(4)—C(5)—N(3)	0(1)	C(6)—N(4)—C(5)—N(3)	179(1)
C(2)—N(4)—C(6)—O(2)	-71(1)	C(5)—N(4)—C(6)—O(2)	111(1)
N(2)—C(2)—C(3)—N(3)	179(1)	N(2)—C(2)—C(3)—C(4)	1(2)
N(4)—C(2)—C(3)—N(3)	-2(1)	N(4)—C(2)—C(3)—C(4)	-179.6(9)
N(3)—C(3)—C(4)—O(1)	6(2)	N(3)—C(3)—C(4)—N(1)	-178(1)
C(2)—C(3)—C(4)—O(1)	-177(1)	C(2)—C(3)—C(4)—N(1)	-1(2)
O(2)—C(7)—C(8)—O(3)	-63(2)	C(9)—C(7)—C(8)—O(3)	54(2)
O(2)—C(7)—C(9)—O(4)	-172.4(8)	C(8)—C(7)—C(9)—O(4)	67(1)

Table 3 Hydrogen bonds. D and A denote the hydrogen donor and acceptor, respectively.

D-H···A	D-H(Å)	H···A(Å)	D···A(Å)	D-H···A(°)
N1-H···N3$^{i)}$	0.96	1.90	2.84(1)	116
N5···O1$^{ii)}$	0.96	1.92	2.85(1)	162
N5···O4$^{ii)}$	0.97	2.28	3.09(1)	141
O4···O1$^{iii)}$	0.82	2.12	2.871(9)	151

Symmetry code: i) (–*x*, –1/2+*y*, –*z*); ii) (2–*x*, –1/2+*y*, 1–*z*); iii) (1+*x*, *y*, 1+*z*).

C9-O4 being 152.7(7), 155.4(8) and –172.4(8)°, respectively. The torsion angle of C2-N4-C6-O2, which determines the relative disposition of the purine ring and the ether oxygen atom, is –71(1)°. The corresponding angle in guanosine determines the relative orientation of the purine and ribose rings, and it is –137.2(8) and –58.1(7)° for crystallographically independent molecules in the crystal structure of guanosine dihydrate. It is interesting to note that the relative orientation of the base ring and the ether oxygen atom in ganciclovir is similar to that observed in one of the independent molecules of guanosine dihydrate. It is likely that the conformation is related to the biological activity of ganciclovir. There are four intermolecular hydrogen bonds, as given in Table 3.

Acknowledgements

This work was supported by Grants for the Key Technology Research Promotion Program of New Energy and Industrial Technology Development Organization (NEDO) of Japan, and also by the Research and Study Program of Tokai University Educational System General Research Organization.

References

1. S. Noble and D. Faulds, *Drugs*, **1998**, *56*, 115.
2. CrystalStructure, version 3.5.1, **2000 – 2003** Crystal Structure Analysis Package, Rigaku and Rigaku/MSC.
3. SIR92: A. Altomare, G. Cascarano, C. Giacovazzo, A. Guagliardi, M. Burla, G. Polidori, and M. Camalli, *J. Appl. Cryst.*, **1994**, *27*, 435.
4. ORTEP III, L. J. Farrugia, *J. Appl. Cryst.*, **1997**, *22*, 389.
5. U. Thewalt, C. E. Bugg, and R. E. Marsh, *Acta Crystallogr., Sect. B*, **1970**, *26*, 1089.

X-ray Structure Analysis Online 2009, VOL. 25

X-ray Structure Analysis Online

Crystal Structure of a Novel Diyne, 1,4-Bis(4-((Z)-1-phenyl-2-(trimethylsilyl)vinyl)phenyl)buta-1,3-diyne

Fumiaki ANZAI,* Takumi KATAISHI,* Taichi NAKANO,* Mieko HIRAYAMA, and Noriaki HIRAYAMA**†**

**Department of Materials Chemistry, School of High-Technology for Human Welfare, Tokai University, 317 Nishino, Numazu, Shizuoka 410-0395, Japan*

***Basic Medical Science and Molecular Medicine, Tokai University School of Medicine, 143 Shimokasuya, Isehara, Kanagawa 259-1143, Japan*

The crystal of the title compound, $C_{38}H_{38}Si_2$, belongs to space group $P\bar{1}$ with cell dimensions of a = 8.6324(6), b = 6.8543(5), c = 27.610(2)Å, α = 89.982(4), β = 89.783(4), and γ = 89.990(5)°. The final R value is 0.057. The central 1,4-diphenylbuta-1,3-diyne moiety takes a linear and planar structure. The trimethylsilyl and the terminal phenyl groups are located on opposite sides with respect to the central planar part.

(Received, October 23, 2008; Accepted March12, 2009; Published on web May 10, 2009)

Organic compounds possessing a high degree of conjugation such as phenylenes or phenyleneethynylenes have long been recognized as ideal materials for advanced electronics and photonic applications such as organic LEDs, liquid crystal displays, and solar cells.[1,2] During a research process of attempting to synthesize X-shaped phenyleneethynylene with terminal vinylsilane units, a novel diyne (1,4-bis(4-((Z)-1-phenyl-2-(trimethylsilyl)vinyl)phenyl)buta-1,3-diyne) was incidentally obtained by a reaction of (Z)-1-(4-ethenylphenyl)-1-phenyl-2-silylethene with 1,2,4,5-tetrabromobenzene. The chemical structure is shown in Fig. 1. An X-ray analysis was undertaken in order to disclose the inherent three-dimensional structure of this novel compound.

Single crystals were obtained from an ethyl acetate-hexane solution. A colorless platelet crystal with a size of 0.38 × 0.35 × 0.10 mm was mounted on a glass fiber and used for data collection. The structure was solved by direct methods and non-H atoms were refined by a full-matrix least-squares method with anisotropic temperature factors. The positions of all H-atoms were located by a difference Fourier synthesis and refined isotropically. The atomic parameters of the H-atoms were fixed in the final refinement. The crystal and experimental data are given in Table 1. The crystal structure shows a symmetry close to space group $P2_1/c$. However, the R_{int} value for the Laue symmetry $2/m$ was 0.042, which is significantly larger than 0.037 for the Laue symmetry $\bar{1}$. In addition, a refinement using space group $P2_1/c$ converged (Δ/σ = 0.000) at a relatively high R factor of 0.075. On the final difference Fourier map significant residual electron densities were observed with $(\Delta\rho)_{max}$ and $(\Delta\rho)_{min}$ being 0.75 and –0.82 e/Å^3, respectively. Therefore we lowered the crystal symmetry to $P\bar{1}$ and it helped with a successful structure refinement.

Two independent molecules located on the center of symmetry are present in an asymmetric unit. The molecular structure of one of the independent molecules, drawn by ORTEP-III, is shown in Fig. 2 with ring labelling. The molecules whose labels

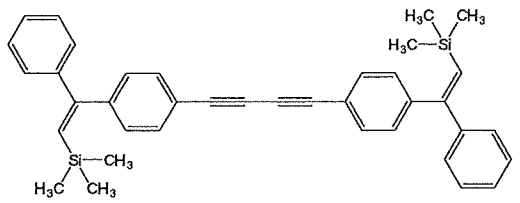

Fig. 1 Chemical structure of 1,4-bis(4-((Z)-1-phenyl-2-(trimethylsilyl)vinyl)phenyl)buta-1,3-diyne.

Table 1 Crystal and experimental data

Formula: $C_{38}H_{38}Si_2$	
Formula weight = 550.89	
Crystal system: triclinic	
Space group: $P\bar{1}$	Z = 2
a = 8.6324(6)Å	α = 89.982(4)°
b = 6.8543(5)Å	β = 89.783(4)°
c = 27.610(2)Å	γ = 89.990(5)°
V = 1633.6(2)Å^3	
D_x = 1.120 g/cm^3	
No. of observations (all) = 3176	
θ_{max} = 68.2° with Cu K_α	
R(all) = 0.057	
$(\Delta/\sigma)_{max}$ = 0.000	
$(\Delta\rho)_{max}$ = 0.15 e/Å^3	
$(\Delta\rho)_{min}$ = –0.17 e/Å^3	
Measurement: Rigaku RAXIS-RAPID	
Program system: CrystalStructure 3.7.0[3]	
Structure determination: SIR92[4]	
Refinement: full-matrix	
CCDC deposition number: 711786	

† To whom correspondence should be addressed.
E-mail: hirayama@is.icc.u-tokai.ac.jp

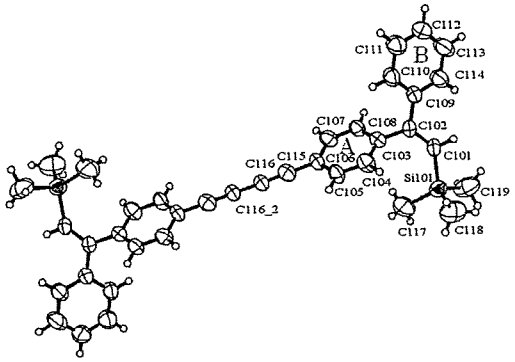

Fig. 2 Molecular structure of 1,4-bis(4-((Z)-1-phenyl-2-(trimethylsilyl)vinyl)phenyl)buta-1,3-diyne along with the atom and ring labelings. Thermal ellipsoids of non-H atoms are drawn at the 50% probability level.

Table 2 Selected bond lengths (Å), bond angles(°) and torsion angles(°)

molecule I		molecule II	
Si(101) - C(101)	1.869(4)	Si(201) - C(201)	1.857(3)
Si(101) - C(117)	1.858(5)	Si(201) - C(217)	1.843(5)
Si(101) - C(118)	1.847(5)	Si(201) - C(218)	1.858(5)
Si(101) - C(119)	1.854(4)	Si(201) - C(219)	1.862(4)
C(101) - C(102)	1.351(6)	C(201) - C(202)	1.347(5)
C(106) - C(115)	1.425(5)	C(206) -C(215)	1.450(5)
C(115) - C(116)	1.213(5)	C(215) - C(216)	1.182(5)
C(116) - C(116)[1]	1.372(5)	C(216) - C(216)[2]	1.394(4)
C(101) - Si(101) - C(117)	115.5(2)	C(201) - Si(201) - C(217)	115.8(2)
C(101) - Si(101) - C(118)	108.1(2)	C(201) - Si(201) - C(218)	108.3(2)
C(101) - Si(101) - C(119)	103.7(2)	C(201) - Si(201) - C(219)	104.3(2)
C(117) - Si(101) - C(118)	110.5(2)	C(217) - Si(201) - C(218)	111.5(2)
C(117) - Si(101) - C(119)	108.2(2)	C(217) - Si(201) - C(219)	107.8(2)
C(118) - Si(101) - C(119)	110.6(2)	C(218) - Si(201) - C(219)	108.8(2)
Si(101) - C(101) - C(102)	134.0(3)	Si(201) - C(201) - C(202)	135.4(2)
C(101)-C(102)-C(103)-C(104)	57.7(5)	C(201)-C(202)-C(203)-C(204)	57.6(5)
C(101)-C(102)-C(109)-C(110)	-152.9(4)	C(201)-C(202)-C(209)-C(210)	-151.8(4)
Si(101)-C(101)-C(102)-C(103)	8.6(6)	Si(201)-C(201)-C(202)-C(203)	9.3(5)
Si(101)-C(101)-C(102)-C(109)	-172.2(3)	Si(201)-C(201)-C(202)-C(209)	-172.2(2)
C(117)-Si(101)-C(101)-C(102)	11.6(5)	C(217)-Si(201)-C(201)-C(202)	12.2(4)
C(118)-Si(101)-C(101)-C(102)	-112.8(4)	C(218)-Si(201)-C(201)-C(202)	-113.8(4)
C(119)-Si(101)-C(101)-C(102)	129.8(4)	C(219)-Si(201)-C(201)-C(202)	130.4(4)

Symmetry operators: (1) $-x, -y+3, -z+1$ (2) $-x+2, -y+2, -z+2$.

are 100s and 200s are designated as molecules I and II, respectively. Selected bond lengths, bond angles and torsion angles are given in Table 2. The 1,4-diphenylbuta-1,3-diyne moiety takes a linear and planar structure. The molecules are centrosymmetric, and hence the trimethylsilyl and the terminal phenyl groups are located on opposite sides with respect to the central 1,3-diyne part. Two independent halves of the molecules take very similar structures. The hundreds of digits of atomic labels are omitted for the sake of simplicity in the following description. The geometrical parameters for molecule I are followed by the corresponding values for molecule II in square brackets. The dihedral angle between two phenyl planes is 106.2(2) [106.2(2)]°. The torsion angle of Si-C1-C2-C3 is 8.6(6) [9.3(5)]°. The trimethylsilyl group faces ring A. The C17 atom points to the center of ring A(Cg) with the C17···Cg distances being 3.71 [3.73]Å. Although the distances are not significantly short, this conformation indicates a weak attractive interaction between ring A and the methyl group. The bond angle of C17-Si-C1 is 115.5(2) [115.8(2)]°, which is significantly larger than the corresponding angles with respect to C18 and C19. The bond angle Si-C1-C2 is 134.0(3) [135.4(2)]°. The widening of these bond angles also suggests an interaction between C17 and ring A. The other bond angles and bond lengths in the molecules are within the expected ranges. The molecules are packed by van der Waals interactions in the crystal.

Acknowledgements

We thank the Research and Study Program of Tokai University Educational System General Research Organization for financial support.

References

1. J. N. Wilson, M. Josowicz, Y. Wang, and U. H. F. Bunz, *Chem. Commun.*, **2003**, 2962.
2. J. Tonggang, L. Yuliang, L. Huibiao, Y. Jianping, L. Xiaofeng, J. Li, Y. Mingjian, L. Junbo, L. Cuihong, W. Shu, and Z. Daoben, *Tetrahedron*, **2007**, *63*, 3168.

X-ray Structure Analysis Online 2009, VOL. 25

X-ray Structure Analysis Online

Crystal Structure of 1,4-Bis[4-((2*Z*)-(trimethylsilyl)-1-phenylethenyl)-phenylethynyl]benzene

Takumi KATAISHI,* Fumiaki ANZAI,* Taichi NAKANO,* Mieko HIRAYAMA, and Noriaki HIRAYAMA**†**

**Department of Materials Chemistry, School of High-Technology for Human Welfare, Tokai University, 317 Nishino, Numazu, Shizuoka 410-0395, Japan*

***Basic Medical Science and Molecular Medicine, Tokai University School of Medicine, 143 Shimokasuya, Isehara, Kanagawa 259-1143, Japan*

The crystal of the title compound, $Si_2C_{44}H_{42}$, belongs to space group $P2_1/c$ with cell dimensions of a = 11.8349(6), b = 8.5746(5), c = 18.6172(10)Å, β = 95.785(3)°. The final $R1$ [$I > 2\sigma(I)$] value is 0.0489. The central conjugated system composed of phenyleneethynylene groups takes a linear, but non-planar structure. The molecule has a center of symmetry. The dihedral angle between the central phenyl ring and the flanking phenyl ring is 18.7(1)°. The two trimethylsilyl groups are located on opposite sides of the molecule with respect to the central part.

(Received, April 9, 2009; Accepted May 29, 2009; Published on web October 10, 2009)

Organic compounds possessing a high degree of conjugation, such as poly(phenyleneethynylene)s, have been recognized as ideal materials for advanced electronic and photonic applications such as for organic LEDs, liquid-crystal displays and solar cells.[1] In aiming to obtain such functional materials, we have been undertaking a series of studies to synthesize a family of novel low-molecular-weight phenyleneethynylenes with terminal vinylsilane units. Although various phenyleneethynylenes have been synthesized, only a few phenyleneethynylenes with terminal vinylsilane unit(s) have been synthesized so far. Recently, we successfully synthesized the title compound (Fig. 1) by the Sonogashira-Hagihara cross-coupling of 1,4-diethynylbenzene with 2 equiv. of (*Z*)-1-(4-iodophenyl)-2-(trimethylsilyl)-1-phenylethene, being prepared by the Migita-Kosugi-Stille cross-coupling of 1,4-di-iodobenzene with (*Z*)-1-(tributylstannyl)-2-(trimethylsilyl)-1-phenylethene,[2] in an isolated yield of 89%. An X-ray analysis was undertaken in order to disclose the inherent three-dimensional structure of this novel compound.

Single crystals were obtained from an ethyl acetate-hexane solution. A colorless platelet crystal with a size of 0.50 × 0.50 × 0.10 mm was mounted on a glass fiber and used for data collection. The structure was solved by direct methods, and non-H atoms were refined by a full-matrix least-squares method with anisotropic temperature factors. The positions of all H-atoms were located by a difference Fourier synthesis and refined by the riding model. In the final refinement, however, the atomic parameters of the H-atoms were fixed. The molecule has a center of symmetry. The crystal and experimental data are

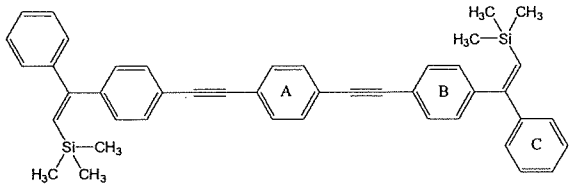

Fig. 1 Chemical structure of 1,4-bis[4-((2*Z*)-(trimethylsilyl)-1-phenylethenyl)phenylethynyl]benzene along with the ring labels.

Table 1 Crystal and experimental data

Chemical formula: $Si_2C_{44}H_{42}$	
Formula weight = 626.99	
T = 296 K	
Crystal system: monoclinic	Space group: $P2_1/c$
a = 11.8349(6)Å	
b = 8.5746(5)Å	β = 95.785(3)°
c = 18.617(1)Å	
V = 1633.6(2)Å^3	Z = 2
D_x = 1.108 g/cm^3	
Radiation: Cu K_α (λ = 1.54187 Å)	
μ(Cu K_α) = 1.056 mm^{-1}	F(0 0 0) = 668
Crystal size = 0.50 × 0.50 × 0.10 mm^3	
No. of reflections collected = 17010	
No. of independent reflections= 3339	
θ_{max} = 67.5° with Cu K_α	
Data/Restraints/Parameters = 3336/0/208	
Goodness-of-fit on F^2 = 0.885	
R indices [$I > 2\sigma(I)$]: $R1$ = 0.0489	
R indices (all data): $R1$ = 0.0549, $wR2$ = 0.1392	
$(\Delta/\sigma)_{max}$ = 0.000	
$(\Delta\rho)_{max}$ = 0.18 e/Å^3	$(\Delta\rho)_{min}$ = –0.40 e/Å^3
Measurement: Rigaku RAXIS-RAPID	
Program system: CrystalStructure 3.7.0[3]	
Structure determination: SIR92[4]	
CCDC deposition number: 726795	

† To whom correspondence should be addressed.
E-mail: hirayama@is.icc.u-tokai.ac.jp

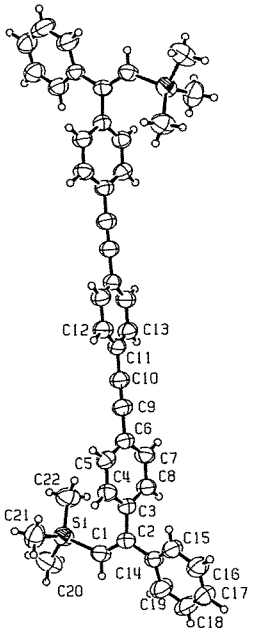

Fig. 2 Molecular structure of 1,4-bis[4-((2Z)-(trimethylsilyl)-1-phenylethenyl)phenylethynyl]benzene along with the atom labels. Thermal ellipsoids of non-H atoms are drawn at the 50% probability level.

given in Table 1.

A stereoscopic drawing of the molecule prepared by ORTEP-III[5] is shown in Fig. 2. Selected bond lengths, bond angles and torsion angles are given in Table 2. The central conjugated system composed of phenyleneethynylene groups take a linear, but non-planar structure. The two trimethylsilyl groups are located on opposite sides of the molecule with respect to the central conjugated part. The dihedral angle between the central phenyl ring A and the flanking phenyl ring B is 18.7(1)°, which indicates that the conjugated system takes an appreciably non-planar structure. The dihedral angle between the terminal phenyl ring C and the rings A and B are 72.4(1) and 90.9(1)°, respectively. The terminal phenyl ring is nearly perpendicular to the ring B. The C1-C2-C3-C4 torsion angle of 68.5(2)° indicates that the silyl group is also significantly deviated from the central conjugated system. The C1-Si-C22 bond angle is 113.86(9)°, and it is significantly larger than those of C1-Si-C20 and C1-Si-C21. The C22 atom points to the center of the ring B(Cg) with the C22···Cg distances being 3.54 Å. It indicates a weak attractive interaction between the ring B and this methyl group. The bond angle of C1-C2-C14 is significantly larger than that of C3-C2-C14, presumably due to a steric repulsion between hydrogen atoms attached to the C1 and C19 atoms with the H···H distance of 2.21 Å. The molecules are packed by van der Waals interactions in the crystal.

Table 2 Selected bond lengths (Å), bond angles (°) and torsion angles (°)

Si(1)-C(1)	1.864(2)	Si(1)-C(20)	1.862(2)
Si(1)-C(21)	1.867(2)	Si(1)-C(22)	1.866(2)
C(2)-C(3)	1.493(2)	C(6)-C(9)	1.437(2)
C(9)-C(10)	1.193(2)	C(10)-C(11)	1.433(2)
C(1)-Si(1)-C(20)	106.5(1)	C(1)-Si(1)-C(21)	109.0(1)
C(1)-Si(1)-C(22)	113.86(9)	C(20)-Si(1)-C(21)	108.9(1)
C(20)-Si(1)-C(22)	108.5(1)	C(21)-Si(1)-C(22)	109.9(1)
Si(1)-C(1)-C(2)	131.49(13)	C(1)-C(2)-C(3)	119.8(1)
C(1)-C(2)-C(14)	123.31(14)	C(3)-C(2)-C(14)	116.8(1)
C(2)-C(14)-C(15)	120.55(15)	C(2)-C(14)-C(19)	122.4(2)
C(6)-C(9)-C(10)	177.4(2)	C(9)-C(10)-C(11)	178.2(2)
C(20)-Si(1)-C(1)-C(2)	155.2(2)	C(21)-Si(1)-C(1)-C(2)	-87.4(2)
C(22)-Si(1)-C(1)-C(2)	35.7(2)	Si(1)-C(1)-C(2)-C(3)	-1.1(2)
Si(1)-C(1)-C(2)-C(14)	176.2(1)	C(5)-C(6)-C(9)-C(10)	-90(4)
C(7)-C(6)-C(9)-C(10)	89(4)	C(6)-C(9)-C(10)-C(11)	-69(9)
C(9)-C(10)-C(11)-C(12)	178(3)	C(9)-C(10)-C(11)-C(13)	-3(4)

Acknowledgements

We thank the Research and Study Program of Tokai University Educational System General Research Organization for financial support.

References

1. T. Jiu, Y. Li, H. Liu, L. Jiang, M. Yuan, J. Li, C. Li, S. Wang, and D. Zhu, *Tetrahedron*, **2007**, *63*, 3168.
2. K. Sonogashira, K. Thoda, and N. Hagihara, *Tetrahedron Lett.*, **1975**, 4467.
3. CrystalStructure, verSion 3.5.1, **2000 – 2003**, Crystal Structure Analysis Package, Rigaku and Rigaku/MSC.
4. SIR92: A. Altomare, G. Cascarano, C. Giacovazzo, A. Guagliardi, M. Burla, G. Polidori, and M. Camalli, *J. Appl. Cryst.*, **1994**, *27*, 435.
5. ORTEP III, L. J. Farrugia, *J. Appl. Cryst.*, **1997**, *22*, 389.

Journal of Cerebral Blood Flow & Metabolism (2009), 1–9

www.jcbfm.com

A novel inhibitor of plasminogen activator inhibitor-1 provides antithrombotic benefits devoid of bleeding effect in nonhuman primates

Yuko Izuhara[1], Nagahisa Yamaoka[2], Hidehiko Kodama[2], Takashi Dan[1], Shunya Takizawa[3], Noriaki Hirayama[4], Kanji Meguro[2], Charles van Ypersele de Strihou[5] and Toshio Miyata[1]

[1]*Center for Translational and Advanced Research, Tohoku University Graduate School of Medicine, Miyagi, Aoba-ku, Sendai, Japan;* [2]*CT Laboratory, Hamari Chemicals Ltd, Osaka, Japan;* [3]*Department of Neurology, Tokai University School of Medicine, Kanagawa, Japan;* [4]*Basic Medical Science and Molecular Medicine, Tokai University School of Medicine, Kanagawa, Japan;* [5]*Service de Nephrologie, Universite Catholique de Louvain, Brussels, Belgium*

Inhibition of plasminogen activator inhibitor (PAI)-1 is useful to treat several disorders including thrombosis. An inhibitor of PAI-1 (TM5275) was newly identified by an extensive study of structure-activity relationship based on a lead compound (TM5007) which was obtained through virtual screening by docking simulations. Its antithrombotic efficacy and adverse effects were tested *in vivo* in rats and nonhuman primates (cynomolgus monkey). TM5275, administered orally in rats (1 to 10 mg/kg), has an antithrombotic effect equivalent to that of ticlopidine (500 mg/kg) in an arterialvenous shunt thrombosis model and to that of clopidogrel (3 mg/kg) in a ferric chloride-treated carotid artery thrombosis model. TM5275 does not modify activated partial thromboplastin time and prothrombin time or platelet activity and does not prolong bleeding time. Combined with tissue plasminogen activator, TM5275 improves the latter's therapeutic efficacy and reduces its adverse effect. Administered to a monkey model of photochemical induced arterial thrombosis, TM5275 (10 mg/kg) has the same antithrombotic effect as clopidogrel (10 mg/kg), without enhanced bleeding. This study documents the antithrombotic benefits of a novel, more powerful, PAI-1 inhibitor in rats and, for the first time, in nonhuman primates. These effects are obtained without adverse effect on bleeding time.
Journal of Cerebral Blood Flow & Metabolism (2009) **0**, 000–000. doi:10.1038/jcbfm.2009.272

Keywords: bleeding; cynomolgus monkey; PAI-1 inhibitor; thrombosis; tissue plasminogen activator

Introduction

Plasminogen activator inhibitor (PAI)-1, a serine protease inhibitor, is involved in numerous processes including thrombosis and fibrosis, as shown by the fact that disruption of the PAI-1 gene in mice markedly attenuates these processes (Carmeliet *et al*, 1993; Eitzman *et al*, 1996, 2000; Weisberg *et al*, 2005; Nicholas *et al*, 2005). Its inhibition may thus yield important cardio- and reno-protective benefits (Ha *et al*, 2009). Recent studies in mice overexpressing human PAI-1 also implicate its involvement in broader biological abnormalities, including alopecia, amyloidosis, and polycystic ovarian syndrome (Eren *et al*, 2007; Devin *et al*, 2007). The availability of specific PAI-1 antagonists may thus open new therapeutic avenues (Vaughan *et al*, 2007).

We have recently developed an original approach to synthesize such orally active inhibitors (Izuhara *et al*, 2008). Compounds selected virtually by structure based drug design underwent a docking simulation to select those which fitted within the cleft of the PAI-1 three-dimensional structure. They inhibit coagulation in two different rodent models of thrombosis and prevent the fibrotic process initiated by bleomycin in mouse lung (Izuhara *et al*, 2008).

This study has been undertaken on a newly synthesized PAI-1 inhibitor (TM5275), to test *in vivo* its antithrombotic efficacy as well as its possible adverse effects. We further assess the clinical benefits of a combination therapy of TM5275 with tissue plasminogen activator (tPA).

Correspondence: Dr T Miyata, Center for Translational and Advanced Research, Tohoku University School of Medicine, 2-1 Seiryo-Machi, Aoba-ku, Sendai 980-8575, Japan.
E-mail: t-miyata@mail.tains.tohoku.ac.jp
Received 7 July 2009; revised 2 December 2009; accepted 9 December 2009

The therapeutic efficacy of TM5275 has been evaluated not only in rodents but also in nonhuman primates as recommended by recent guidelines (STAIR, 1999) to reduce discrepancies between preclinical animal trials and clinical studies. Indeed, the pathophysiological mechanisms involved in the development of thrombosis in preclinical rodent models may differ from those implicated in primates, including man (STAIR, 1999). TM5275 proves an effective antithrombotic agent which spares activated partial thromboplastin time/prothrombin time and platelet activity and does not prolong bleeding time. Combined with tPA, it improves the latter's therapeutic efficacy and reduces its adverse effects.

This study is the first to demonstrate in nonhuman primates that PAI-1 inhibition reduces markedly vascular thrombosis without modification of bleeding time, which is the most critical adverse effect of various antithrombotic agents.

Materials and methods

Synthesis of Test Compounds

More than ninety novel compounds (2-acylamino-3-thiophenecarboxylic acid and 2-acylaminobenzoic acid derivatives with comparatively low molecular weights (400 to 550) and without symmetrical structure, designed based on the original PAI-1 inhibitor TM5007 (Izuhara *et al*, 2008)) as well as PAI-749 (Gardell *et al*, 2007), a previously reported PAI-1 inhibitor, were synthesized by Hamari Chemicals Ltd (Osaka, Japan). They were screened *in vitro* for PAI-1 inhibitory activity.

Docking Simulations

Docking simulations were undertaken by the program ASEDock (Goto *et al*, 2008). The crystal structure of a complex between PAI-1 and the inhibitory reactive-center loop peptide (1A7C) was obtained from the Protein Data Bank (Bernstein *et al*, 1997) and used as the target structure for the docking simulations.

In Vitro PAI-1 Activity Assay

PAI-1 inhibitory activity was assessed by a previously described chromogenic assay (Izuhara *et al*, 2008). The composition of the incubation medium was adapted to increase the assay's sensitivity: 0.15 mol/L NaCl, 50 mmol/L Tris-HCl pH8, 0.2 mmol/L CHAPS, 0.1% PEG-6000, 1% dimethylsulfoxide, 5 nmol/L human active PAI-1, 2 nmol/L human 2-chain tPA and 0.2 mmol/L Spectrozyme tPA at final concentration. Tested compounds were added at various concentrations and the IC_{50} was calculated by logit-log analysis.

PAI-1/tPA Complex on Sodium Dodecyl Sulfate-Polyacrylamide Gel Electrophoresis

The effect of the tested compound on the formation of a PAI-1/tPA complex was estimated in an incubation medium mixing PAI-1, tPA, and the compound. The eventual composition included 100 mmol/L HEPES, pH 7.4, 150 mmol/L NaCl, 0.05% Tween 20, 0.8% dimethylsulfoxide, 0.875 μmol/L PAI-1, 0.7 μmol/L tPA, and compound (160 μmol/L). Proteins were separated by sodium dodecyl sulfate-polyacrylamide gel electrophoresis and visualized by Coomassie staining.

Pharmacokinetic Studies

Animal experiments were performed in accordance with the Animal Experimentation Guidelines of Tokai University School of Medicine. TM5275, suspended in 0.5% carboxymethyl cellulose sodium salt (CMC) solution, was administered orally by gavage to male ICR mice (50 mg/kg) (CLEA Japan Inc., Tokyo, Japan), male Wistar rats (50 mg/kg) (CLEA Japan Inc.), and male cynomolgus monkeys (1 mg/kg) (Macaca Fascicularis) (Japan SLC, Shizuoka, Japan). Heparinized blood samples were collected from the vein before (0 h) and 1, 2, 6, and 24 h after oral drug administration. Plasma drug concentration was determined on a reverse-phase high-performance liquid chromatography. Maximum drug concentration time (T_{max}), maximum drug concentration (C_{max}), and drug half-life ($T_{\frac{1}{2}}$) were then calculated. For the BA study in monkeys, heparinized blood samples were collected from the vein before (0 h) and 0.5, 1, 2, 4, 6, 8, 24, 48, 72, 120, and 168 h after oral drug administration, and before (0 h) and 0.08, 0.25, 0.5, 1, 2, 4, 6, 8, 24, 48, 72, 120, and 168 h after intravenous drug injection. BA was calculated by non-compartment model analysis using WinNonlin Professional Software, version 5.01 (Pharsight Co., NC, USA).

Toxicity

All toxicity studies followed the International Conference on Harmonisation of Technical Requirements for Registration of Pharmaceuticals for Human Use (ICH) Harmonised Tripartite Guidelines at the non-GLP conditions.

For the evaluation of acute toxicity, TM5275 (1000 mg/kg for mice and 2000 mg/kg for rats and monkeys), suspended in 0.5% CMC solution, was administered orally by gavage to male ($n=5$) and female ($n=5$) ICR mice (CLEA Japan Inc.), male ($n=5$) and female ($n=5$) Sprague–Dawley rats (Charles River Japan Inc., Kanagawa, Japan), and male cynomolgus monkeys ($n=2$) (Japan SLC). The animal's body weight was monitored once a week. Various organs underwent histological studies 2 weeks (mice) and 1 week (rats) after drug administration.

For the evaluation of the subacute toxicity, three different doses of TM5275 (200, 600, and 2000 mg/kg/day) were administered for 2 weeks by gavage to male ($n=5$) and female ($n=5$) Sprague–Dawley rats (Charles River Japan) and male cynomolgus monkeys ($n=2$) (Japan SLC). At the end of the study, blood glucose, total cholesterol, triglyceride, aspartate aminotransferase, alanine aminotransferase, creatinine, urea nitrogen, total protein, albumin, hemoglobin, red blood cells, and hematocrit levels as well as activated partial thromboplas-

tin time and prothrombin time were assessed. Body weight was measured and urinary analysis performed.

The following safety pharmacology core battery was used: a modified Irwin's test for the central nervous system in Sprague–Dawley rats dosing TM5275 up to 2 g/kg *per* os, and three cardiovascular tests. (1) QT interval in telemetry electrocardiogram recording in beagle dogs administered an oral dose of 2 g/kg of TM5275; (2) action potentials of guinea-pig right ventricular papillary muscles at a dose of 5 μmol/L of TM5275; and (3) hERGIkr current measured in stably transfected human embryonic kidney (HEK) 293 cells at a dose of 5 μmol/L of TM5275.

Arteriovenous Shunt Thrombosis Rat Model

Thrombus formation in arteriovenous shunts was achieved in male CD rats (Charles River Japan) by a previously described method (Morishima *et al*, 1997). Either TM5275 (10 and 50 mg/kg, $n=9$) or ticlopidine (500 mg/kg, $n=6$: Wako Pure Industries Ltd, Osaka, Japan), suspended in 0.5% CMC solution, was administered orally by gavage 90 mins before the study. Control rats were administered only a 0.5% CMC solution ($n=10$). Blood was allowed to circulate through the shunt for 30 mins. The wet weight of the thrombus covering the silk thread was eventually measured.

Ferric Chloride-Treated Carotid Artery Thrombosis Rat Model

Male Sprague–Dawley rats weighing 280 to 310 g (Japan SLC) were anesthetized with pentobarbital sodium (50 mg/kg, intraperitoneally) and fixed on a heating pad. During the experiment, rectal temperature was maintained at 38°C. The left common carotid artery was exposed, and a piece of filter paper (2.5 × 4.2 mm) was folded around it. The probe of a pulsed Doppler flowmeter (Model PDV-20, Crystal Biotech America, Hopkinton, MA, USA) was placed to measure the arterial blood flow. After obtention of a steady baseline flow, 2 μL of ferric chloride ($FeCl_3$) saline solution (35% (w/w)) was added to the filter paper. Five minutes later, the filter paper was removed and the artery washed with saline. Blood flow in the common carotid artery was continuously monitored for 30 mins after $FeCl_3$ saline exposure. Time to primary occlusion was calculated.

Several concentrations of TM5275 (0.3, 1, 5 mg/kg) and clopidogrel (1, 3, 10 mg/kg) (Sanofi Aventis, Tokyo, Japan), suspended in 0.5% CMC solution, were administered orally by gavage ($n=8$, each group) 2 h before $FeCl_3$ exposure. After a 30 mins blood flow monitoring, a sphygmomanometer cuff was placed on the tail and inflated to 40 mm Hg. An incision was made with an animal lancet (Goldenrod, Medipoint Inc., Mineola, NY, USA) and, every 30 secs, a wick of filtration paper was inserted on the wound until no further staining was observed. Bleeding time was determined to the nearest 30 secs. If it lasted more than 10 mins, the experiment was discontinued.

The benefits of combining TM5275 with tPA were further ascertained. Either TM5275 (5 mg/kg, $n=10$), tPA (0.3 or 3 mg/kg, $n=10$ each: Kyowa Hakko Kirin Co. Ltd), or TM5275 (5 mg/kg) plus tPA (0.3 mg/kg) ($n=10$) were administered orally (TM5275) or intravenously (tPA). The experiments were performed along the conditions described above.

Photochemically Induced Arterial Thrombosis Monkey Model

Three- to 4-year-old male cynomolgus monkeys (Japan SLC) weighing 2.8 to 3.5 kg underwent anesthesia by an intramuscular injection of 10 mg/kg ketamine hydrochloride followed by the intravenous injection of 25 mg/kg pentobarbital sodium. Animals were fixed on a heating pad, and rectal temperature was maintained at 36.5 to 37.5°C. The saphenous artery was exposed by a 2 cm incision and thrombosis was induced by a photochemical reaction according to the modified method of Umemura *et al* (1993). Briefly, the saphenous artery was irradiated with green light (wave length 540 nm, 900,000 lx) generated by a xenon lamp (L4887, Hamamatsu Photonics, Shizuoka, Japan) with a heat-absorbing filter and a green filter. Irradiation was directed by a 3-mm diameter optic fiber mounted on a micromanipulator. The probe of a pulsed Doppler flowmeter (Model PDV-20, Crystal Biotech America) was placed on the saphenous artery to measure arterial blood flow. Once the baseline flow was steady, a 20 mins photo-irradiation was undertaken and a 6 mins intravenous rose bengal (20 mg/kg) injection initiated. TM5275 (10 mg/kg) or clopidogrel (10 mg/kg) suspended in 0.5% CMC solution were administered by gavage ($n=6$, each group) 2 h before photochemical thrombosis. Blood flow of the saphenous artery was monitored for 3 h after the start of photo-irradiation. In monkeys, in contrast with rodents, photochemically induced arterial thrombosis progressively reduced cerebral blood flow, and was followed by recanalization and eventually by rethrombosis, a sequence observed in stroke patients and called cyclical flow reduction (Maeda *et al*, 2005*a*, *b*). Therefore, total occlusion time was calculated during the experiment.

Bleeding time was measured in monkeys previously acclimated to chair restraint during repeated training sessions several times before the experiment. A sphygmomanometer cuff, placed on the upper leg of conscious monkeys fixed to a monkey chair, was inflated to 40 mm Hg. TM5275 (50 mg/kg) or clopidogrel (10 mg/kg) suspended in 0.5% CMC solution were administered orally by gavage ($n=3$, each group) 2 h before the study. Bleeding was produced inside the lower leg by a Micro Lancet (Abbot Japan, Tokyo, Japan) with a 21-gauge needle. Every 10 sec, a wick of filtration paper was placed on the wound until no further staining was observed. Bleeding time was determined to the nearest 10 secs. Maximum observation period was 10 mins.

Statistics

All data are expressed as the mean ± s.e. Comparisons between two groups were performed using an unpaired *t*-test. For multiple comparisons, one-way analysis of

variance and Dunnett's *post hoc* test were performed. The effect of TM5275 combined with tPA in the $FeCl_3$ model was performed by one-way analysis of variance followed by Bonferroni's multiple comparisons. Values are considered significant at $P<0.05$. All statistical analyses were performed on the statistical package SPSS for Windows (Version 15.0, SPSS, Chicago, IL, USA).

Results

TM5275

TM5275, 5-chloro-2-[({2-[4-(diphenylmethyl) piperazin-1-yl]-2-oxoethoxy}acetyl)amino]benzoate (Figure 1B), was discovered through an extensive structure-activity relationship study with more than 90 compounds designed and synthesized on the basis of the structure of TM5007 (Figure 1A). TM5275 was eventually selected as the test compound after taking into consideration the *in vitro* PAI-1 inhibitory activity and pharmacokinetic studies (T_{max}, C_{max}, $T_{\frac{1}{2}}$) (see below).

The PAI-1 inhibitory activity of TM5275, measured by tPA-dependent hydrolysis of peptide substrate, is comparable to that of TM5007 and PAI-749: Half-maximal inhibition (IC_{50}) values of TM5275, TM5007, and PAI-749 are 6.95, 5.60, and 8.37 μmol/L, respectively.

Docking simulation of the PAI-1 moiety and TM5275 was undertaken to understand the mechanism of TM5275 action. TM5275 binds to strand 4 of the A β-sheet (s4A) position of PAI-1. Although both TM5275 and TM5007 bind within the cleft to the s4A segment of PAI-1, closer inspection reveals that their binding sites differ, as illustrated in Figure 2: the bulky diphenylmethyl group of TM5275 cannot be accommodated to the binding site of TM5007, so that TM5275 is markedly shifted in the s4A cleft.

In vitro, TM5275 (up to 100 μmol/L) does not interfere with other serpin/serine protease systems (that is, $alpha_1$-antitrypsin/trypsin and $alpha_2$-antiplasmin/plasmin). Its PAI-1 inhibitory activity thus appears specific. On sodium dodecyl sulfate-polyacrylamide gel electrophoresis, the PAI-1 covalent complex formed with tPA is not observed when PAI-1 is preincubated with TM5275 (data not shown).

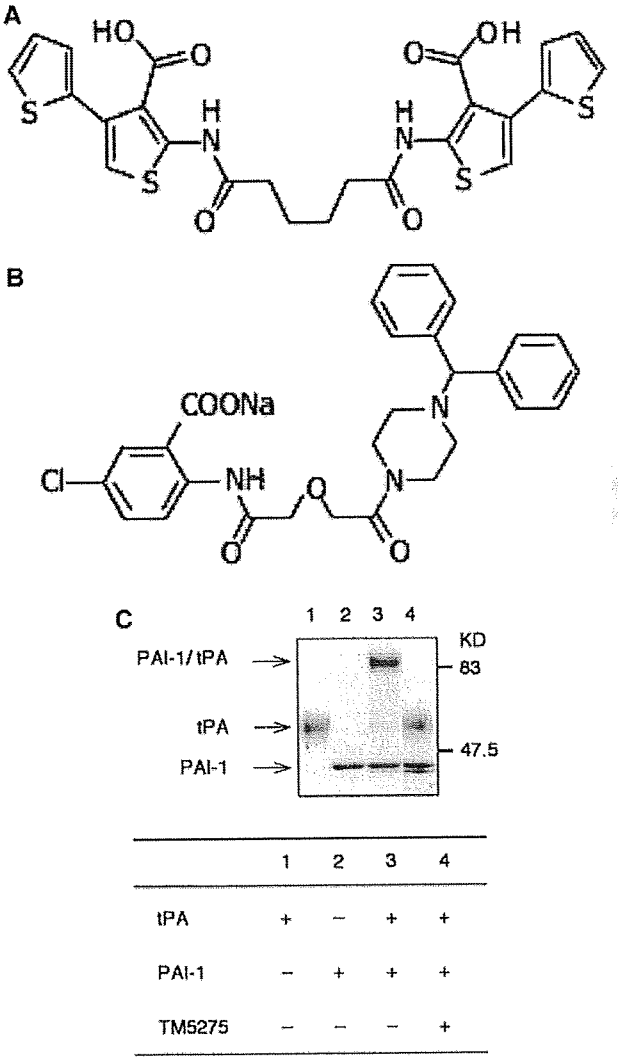

Figure 1 Chemical structures of TM5007 (**A**) and TM5275 (**B**). Molecular weights for TM5007 and TM5275 are 560.02 and 543.97, respectively. On SDS-PAGE (**C**), PAI-1 formed a covalent complex with tPA, whereas no PAI-1/tPA complex formation was observed when PAI-1 was preincubated with TM5275.

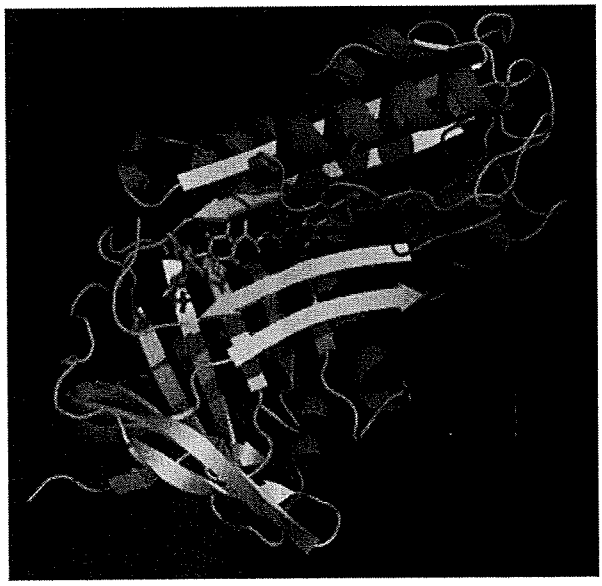

Figure 2 The binding modes of TM5007 (cyan) and TM5275 (pink) obtained by docking simulations are shown. Figures were drawn by a software PyMOL version 0.97 (DeLano Scientific LLC, San Carlo, CA, USA).

Pharmacokinetics

The pharmacokinetics of TM5275 improved significantly when compared with that of TM5007. An oral dose of 50 mg/kg of TM5275, administered in rats, yields calculated plasma T_{max}, C_{max}, and $T_{\frac{1}{2}}$ of 2 h, 34 μmol/L, and 2.5 h, respectively, versus 18 h, 8.8 μmol/L, and 124 h, respectively, in rats administered the same dose of TM5007. TM5275 thus increases C_{max} fourfold, and markedly shortens both T_{max} and $T_{\frac{1}{2}}$. In mice, an oral dose of 50 mg/kg of TM5275 yields the following values for these parameters: 1 h, 6.9 μmol/L, and 6.5 h, respectively. In monkeys, an oral dose of 1 mg/kg of TM5275 yields T_{max}, C_{max}, and $T_{\frac{1}{2}}$ values of 6 h, 10.5 μmol/L, and 114.7 h, respectively. Bioavailability of TM5275 reaches 96% in monkeys.

Toxicity

Acute toxicity has been evaluated *in vivo*. A single dose of TM5275 of 1000 mg/kg in mice and 2000 mg/kg in rats and monkeys elicited no symptoms after 2 weeks in the former group and after 1 week in the latter two groups. Body weight and the histology of various organs are not modified.

Subacute toxicity has been assessed in rats and monkeys administered daily three different doses of TM5275 (200, 600, and 2000 mg/kg/day) for 2 weeks. Body weight and the histology of various organs are not modified. No abnormality is noted in the biochemistry of plasma and urine, including activated partial thromboplastin time, prothrombin time, and red blood cell count.

In safety pharmacology studies, TM5275 does not modify tests of the central nervous system (a modified Irwin's test in rats) or of the cardiovascular system: (1) QT interval in electrocardiogram recording in dogs; (2) action potentials of guinea-pig right ventricular papillary muscles; and (3) hERGIkr current in HEK293 cells.

Rat Thrombosis Models

The antithrombotic effectiveness of TM5275 in a rat arteriovenous shunt model is described in Table 1. Blood clot weights are significantly lower in rats administered 10 and 50 mg/kg of TM5275 (60.9 ± 3.0 and 56.8 ± 2.8 mg, respectively) than in vehicle-treated rats (72.5 ± 2.0 mg). Up to 300 mg/kg of TM5007 are needed to reach the efficacy of 50 mg/kg of TM5275 in the same model. The antithrombotic effectiveness of TM5275 (50 mg/kg) is equivalent to that of ticlopidine (500 mg/kg), a reference antithrombotic compound. Plasma concentration of TM5275 reaches 17.5 ± 5.2 μmol/L after a dose of 10 mg/kg.

The antithrombotic effectiveness of TM5275 in a rat $FeCl_3$ carotid artery thrombosis model is illustrated in Figure 3. TM5275 and clopidogrel, another standard antithrombotic drug, prove antithrombotic in a dose-dependent manner (Figure 3). The minimum effective doses of TM5275 and clopidogrel are 1 and 3 mg/kg, respectively. It corresponds to a TM5275 plasma concentration of 4.9 ± 3.6 μmol/L. As expected, clopidogrel prolongs bleeding time in a dose-dependent manner (Figure 3). By contrast, TM5275 does not affect bleeding time, a potential benefit as an antithrombotic agent. Two hours after oral administration, TM5275 (10 mg/kg) does not affect platelet aggregation induced by ADP and collagen (data not shown). Its antithrombotic effect is thus independent of any effect on platelets.

Table 1 Effect of TM5275 on thrombus weight in a rat arteriovenous shunt model

Treatment	N	*Thrombus weight subtracting thread (mg)*
Vehicle		
0.5% Carboxymethyl cellulose sodium salt (*per* os)	10	72.5 ± 2.0
TM5275		
10 mg/kg (*per* os)	9	60.9 ± 3.0*
50 mg/kg (*per* os)	9	56.8 ± 2.8†
Ticlopidine		
500 mg/kg (*per* os)	6	51.8 ± 2.2†

Data are expressed as mean ± s.e. *$P < 0.01$, †$P < 0.001$ versus vehicle.

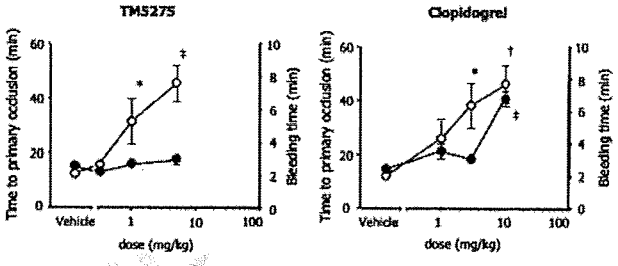

Figure 3 Effects of TM5275 and clopidogrel on primary occlusion time (open circles) and bleeding time (closed circles) in the rat $FeCl_3$-induced thrombosis model. *$P < 0.05$, †$P < 0.01$, ‡$P < 0.001$ versus vehicle. $n = 8$, each group.

TM5275 has been further combined with tPA in the same model, as illustrated in Figure 4. tPA (0.3 mg/kg) alone does not provide a significant antithrombotic effect. However, TM5275 (5 mg/kg) combined with tPA (0.3 mg/kg) significantly enhances the antithrombotic effect of tPA (0.3 mg/kg) alone and provides a benefit similar to that of a high tPA dose (3 mg/kg). The bleeding time of the combination therapy is similar to that of a low tPA dose (0.3 mg/kg) alone.

Monkey Thrombosis Model

The antithrombotic effect of TM5275 has been evaluated in a cynomolgus monkey model of photo-

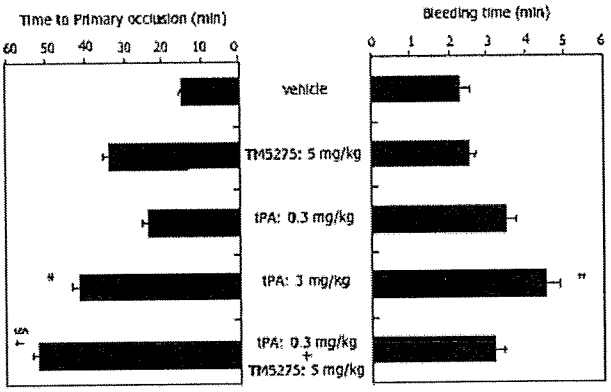

Figure 4 Effect of combination of TM5275 and tPA on primary occlusion time (left panel) and bleeding time (right panel) in the rat $FeCl_3$-induced thrombosis model. $^*P < 0.05$, $^\dagger P < 0.01$, $^\ddagger P < 0.001$ versus vehicle, $^\S P < 0.05$ versus tPA (0.3 mg/kg) alone. $n = 10$, each group.

Table 2 Effect of TM5275 on total occlusion time in the monkey photochemically induced thrombosis model

Treatment	N	*Total occlusion time (min)*
Vehicle 0.5% Carboxymethyl cellulose sodium salt (*per* os)	6	119.0 ± 17.4
Clopidogrel 10 mg/kg (*per* os)	6	39.4 ± 25.8*
TM5275 10 mg/kg (*per* os)	6	53.9 ± 19.9*

Total occlusion time was calculated during the experiment. Data are expressed as mean ± s.e. *$P < 0.05$ versus vehicle.

chemically induced thrombosis (Table 2). Total occlusion time is significantly reduced in both the TM5275 (53.9 ± 19.9 mins) and clopidogrel (39.4 ± 25.8 mins) groups (10 mg/kg, each) in comparison with the vehicle group (119.0 ± 17.4 mins). Plasma concentration of TM5275 reaches 18.9 ± 3.7 μmol/L in the TM5275 group.

The benefits of TM5275, as an antithrombotic agent devoid of effects on bleeding time, have been confirmed in nonhuman primates (Table 3). Two hours after administration of 50 mg/kg (five times higher than the effective dose) of TM5275, the bleeding time is only slightly longer (146.7 ± 3.3 secs) than before administration (83.3 ± 6.7 secs), whereas it is markedly extended in the 10 mg/kg clopidogrel group (>600 secs) above that observed before administration (113.3 ± 8.8 secs).

Table 3 Effect of TM5275 on bleeding time in the monkey photochemically induced thrombosis model

Treatment	N	*Bleeding time (secs)*	
		Before administration	*After administration*
Clopidogrel 10 mg/kg (*per* os)	3	113.3 ± 8.8	>600
TM5275 50 mg/kg (*per* os)	3	83.3 ± 6.7	146.7 ± 3.3

Data are expressed as mean ± s.e.

Discussion

In contrast with a previous rather inefficient high-throughput random screening approach of a large chemical library, we recently reported a novel method to identify small molecular PAI-1 inhibitors, that is, structure-based drug design relying on the virtual screening of small compounds based on the PAI-1 three-dimensional structure (Izuhara *et al*, 2008). Two small molecular PAI-1 inhibitors, TM5001 and TM5007, were thus synthesized and their antithrombotic activity documented in rats (Izuhara *et al*, 2008). In this study, we use the same approach and synthesize a new, more effective PAI-1 inhibitor, TM5275. We show its antithrombotic efficacy not only in rodents but also in monkeys, a more human relevant model.

In limited toxicology studies performed so far, TM5275 appears to be nontoxic. Single doses of 1.0 to 2.0 g/kg elicit no abnormality in rodents or monkeys. Daily doses of 200, 600, or 2000 mg/kg administered for 2 weeks to rats or monkeys also fail to produce symptoms, biochemical disorders, or histological abnormalities in tested organs. More pointed safety pharmacologic tests disclose no neural or cardiovascular toxicity.

Of major interest, TM5275 is 6 times more effective than TM5007: at a dosage of 50 mg/kg, its antithrombotic activity, in a rat arteriovenous shunt model, is equivalent to that obtained by 300 mg/kg of TM5007. This difference is best accounted for by a higher plasma drug concentration of TM5275 reached within 2 h after a 50 mg/kg oral dose, that is, 22.4 μmol/L versus only 5.2 μmol/L after a 300 mg/kg oral dose of TM5007. It fits with the different pharmacokinetic profiles of both drugs: a higher T_{max} reached within a shorter delay after TM5275 (34 μmol/L within 2 h) than after TM5007 (8.8 μmol/L within 18 h). $T_{\frac{1}{2}}$ is more rapid for TM5275 (2.5 h) than for TM5007 (124 h). Interestingly, a lower oral dose of 10 mg/kg administered to nonhuman primates results in intermediary values: T_{max} of 10.5 μmol/L reached within 6 h with a $T_{\frac{1}{2}}$ of 114.7 h. These characteristics argue in favor of oral TM5275 to prevent or dissolve clots in humans, a conclusion further supported by the very high bioavailability of oral TM5275 in monkeys (96%).

Clearly, TM5275 is effective in the prevention of thrombosis in rat models: it dose-dependently

reduces blood clot weight and, at the higher 50 mg/kg doses, is equivalent to a single dose of 500 mg/kg of ticlopidine. In the $FeCl_3$ carotid artery thrombosis model, it (1 mg/kg) also prolongs occlusion time to an extent similar to that of clopidogrel (3 mg/kg) but, unlike the latter, without increasing the bleeding time. In monkeys, the benefits of TM5275 (10 mg/kg) are also apparent as total occlusion time is markedly attenuated to a degree similar to that achieved by clopidogrel (10 mg/kg), but, in contrast to the latter, with only a minor increase in bleeding time.

The differences observed between rodents and monkeys, in TM5275 pharmacokinetics and antithrombotic effects, fully support the recent guidelines (STAIR, 1999) advocating tests in nonhuman primates to reduce discrepancies between preclinical models (usually rodents) and human clinical data. In contrast to rodent thrombosis models, the photochemically induced arterial thrombosis developed in monkeys shows a cyclical flow reduction, that is, a progressive decrease in blood flow with rethrombosis followed by recanalization closely resembling human cerebral thrombosis (Maeda *et al*, 2005*a*, *b*). This difference might reflect specific platelet and coagulation systems. In this nonhuman primate model, TM5275 provides a powerful antithrombotic effect without adverse effects on bleeding time, suggesting its potential benefit, for example, combination therapy with tPA, post-tPA therapy to avoid arterial reocclusion (Alexandrov and Grotta, 2002), treatment for patients with cerebral microbleeds (Nighoghossian *et al*, 2002; Wong *et al*, 2003), or intracranial branch atheromatous disease (Caplan, 1989).

Although tPA has recently become the most effective therapeutic agent for acute ischemic stroke (The National Institute of Neurological Disorders and Stroke rt-PA Stroke Study Group, 1995), symptomatic intracranial hemorrhage remains the most serious, concurrent complication associated with tPA treatment (Derex and Nighoghossian, 2008). In The National Institute of Neurological Disorders and Stroke tPA trial (1995), 6.4% of patients showed a symptomatic intracranial hemorrhage with deterioration of the clinical status in the tPA group, compared with 0.6% in the placebo group. The mortality rate in cases with symptomatic intracranial hemorrhage reached up to 47% (The National Institute of Neurological Disorders and Stroke rt-PA Stroke Study Group, 1997). Recently, an increased risk of intracranial hemorrhage in patients receiving tPA, assessed by concomitant cerebral microbleeding on T2*-weighted magnetic resonance imaging, has been pointed out (Nighoghossian *et al*, 2002), and an alternative thrombolytic therapy without inducing worrisome bleeding disorders often encountered with tPA therapy is expected. We show that, in rats, TM5275 augments its antithrombotic efficacy: added to a standard intravenous dose of tPA (0.3 mg/kg), it more than doubles ($P<0.05$ versus 0.3 mg/kg tPA alone) its time to primary occlusion without increasing bleeding time. Conversely, tPA (3 mg/kg) significantly prolongs the TM5275-induced time to primary occlusion with a small but significant increase in bleeding time. It is noted that the TM5275-tPA (0.3 mg/kg) combination, compared with a 10 times higher dose of injected tPA (3 mg/kg), achieves a longer time to primary occlusion ($P<0.01$ versus vehicle) with a decreased bleeding time. These data obtained in rats suggest that an appropriate combination of oral TM5275 with intravenous tPA might prove valuable in clinical emergencies without inducing worrisome bleeding disorders.

Clinical deterioration after tPA therapy was observed in the National Institute of Neurological Disorders and Stroke rt-PA Stroke Study (Grotta *et al*, 2001), and early cerebral arterial reocclusion occurs in 34% of tPA-treated patients with any initial recanalization (Alexandrov and Grotta, 2002). Oral administration of TM5275, followed by intravenous tPA treatment, may be beneficial. Also, the presence of cerebral microbleeds on T2*-weighted magnetic resonance imaging has been pointed out as a marker of increased risk of intracranial hemorrhage in patients receiving tPA (Nighoghossian *et al*, 2002) or taking aspirin (Wong *et al*, 2003). An alternative thrombolytic and/or antiplatelet therapy without inducing worrisome bleeding disorders, such as TM5275, may therefore provide benefits. Q3

Intracranial branch atheromatous disease is another candidate for TM5275 treatment. Patients with atheromatous disease of an arterial branch present a gradual or stepwise progression of clinical signs, because platelet-fibrin plugs may form, break off, and embolize distally (Caplan, 1989), a mechanism mimicking the cyclical flow reduction by the photochemically induced arterial thrombosis (Maeda *et al*, 2005*a*, *b*) shown in our study using cynomolgus monkeys.

Several characteristics of TM5275 might prove helpful in the treatment of thrombotic disorders. First of all, unlike other types of antithrombotic agents for example, anticoagulation or antiplatelet agents), it does not prolong bleeding time and has virtually no influence on activated partial thromboplastin time/prothrombin time and platelet activity. Second, its impressive bioavailability warrants an administration *per* os, a substantial advantage over tPA. The demonstration that, combined with the latter, it enhances its activity supports a joint administration.

It is noteworthy that inhibition of PAI-1 in humans may not induce serious adverse effects. Currently, two genetic defects in the PAI-1 gene have been documented in humans (Mehta and Shapiro, 2008). Affected individuals do have a mild bleeding tendency but rarely exhibit severe bleeding events commonly seen in other procoagulant deficiencies: most episodes are post-traumatic or post-surgical. The majority of bleeding events are controlled with

antifibrinolytic agents, such as tranexamic acid and ε-aminocaproic acid. In PAI-1-deficient patients, a normal lifespan is achieved. Further clinical studies are needed to support these conclusions.

Acknowledgements

This study was supported by a grant from the New Energy and Industrial Technology Development Organization in Japan (to TM and NH).

Conflict of interest

The authors declare no conflict of interest.

References

Alexandrov AV, Grotta JC (2002) Arterial reocclusion in stroke patients treated with intravenous tissue plasminogen activator. *Neurology* 59:862–7

Bernstein FC, Koetzle TF, Williams GJ, Meyer EF, Jr, Brice MD, Rodgers JR, Kennard O, Shimanouchi T, Tasumi M (1997) The protein data bank: a computer-based archival file for macromolecular structures. *J Mol Biol* 112:535–42

Caplan LR (1989) Intracranial branch atheromatous disease: a neglected, understudied, and underused concept. *Neurology* 39:1246–50

Carmeliet P, Stassen JM, Schoonjans L, Ream B, van den Oord JJ, De Mol M, Mulligan RC, Collen D (1993) Plasminogen activator inhibitor-1 gene-deficient mice: II. Effects on hemostasis, thrombosis, and thrombolysis. *J Clin Invest* 92:2756–60

Derex L, Nighoghossian N (2008) Intracerebral haemorrhage after thrombolysis for acute ischaemic stroke: an update. *J Neurol Neurosurg Psychiatry* 79:1093–9

Devin JK, Johnson JE, Eren M, Gleaves LA, Bradham WS, Bloodworth JR, Jr, Vaughan DE (2007) Transgenic overexpression of plasminogen activator inhibitor-1 promotes the development of polycystic ovarian changes in female mice. *J Mol Endocrinol* 39:9–16

Eitzman DT, McCoy RD, Zheng X, Fay WP, Shen T, Ginsburg D, Simon RH (1996) Bleomycin-induced pulmonary fibrosis in transgenic mice that either lack or overexpress the murine plasminogen activator inhibitor-1 gene. *J Clin Invest* 97:232–7

Eitzman DT, Westrick RJ, Xu Z, Tyson J, Ginsburg D (2000) Plasminogen activator inhibitor-1 deficiency protects against atherosclerosis progression in the mouse carotid artery. *Blood* 96:4212–5

Eren M, Gleaves LA, Atkinson JB, King LE, Declerck PJ, Vaughan DE (2007) Reactive site-dependent phenotypic alterations in plasminogen activator inhibitor-1 transgenic mice. *J Thromb Haemost* 5:1500–8

Gardell SJ, Krueger JA, Antrilli TA, Elokdah H, Mayer S, Orcutt SJ, Crandall DL, Vlasuk GP (2007) Neutralization of plasminogen activator inhibitor 1 (PAI-1) by the synthetic antagonist PAI-749 via a dual mechanism of action. *Mol Pharmacol* 72:897–906

Goto J, Kataoka R, Muta H, Hirayama N (2008) ASEDock-docking based on alpha spheres and excluded volumes. *J Chem Inf Model* 48:583–90

Grotta JC, Welch KM, Fagan SC, Lu M, Frankel MR, Brott T, Levine SR, Lyden PD (2001) Clinical deterioration following improvement in the NINDS rt-PA Stroke Trial. *Stroke* 32:661–8

Ha H, Oh EY, Lee HB (2009) The role of plasminogen activator inhibitor 1 in renal and cardiovascular diseases. *Nat Rev Nephrol* 5:203–11

Izuhara Y, Takahashi S, Nangaku M, Takizawa S, Ishida H, Kurokawa K, van Ypersele de Strihou C, Hirayama N, Miyata T (2008) Inhibition of plasminogen activator inhibitor-1: its mechanism and effectiveness on coagulation and fibrosis. *Arterioscler Thromb Vasc Biol* 28:672–7

Maeda M, Moriguchi A, Mihara K, Aoki T, Takamatsu H, Matsuoka N, Mutoh S, Goto T (2005a) FK419, a nonpeptide platelet glycoprotein IIb/IIIa antagonist, ameliorates brain infarction associated with thrombotic focal cerebral ischemia in monkeys: comparison with tissue plasminogen activator. *J Cereb Blood Flow Metab* 25:108–18

Maeda M, Takamatsu H, Furuichi Y, Noda A, Awaga Y, Tatsumi M, Yamamoto M, Ichise R, Nishimura S, Matsuoka N (2005b) Characterization of a novel thrombotic middle cerebral artery occlusion model in monkeys that exhibits progressive hypoperfusion and robust cortical infarction. *J Neurosci Methods* 146:106–15

Mehta R, Shapiro AD (2008) Plasminogen activator inhibitor type 1 deficiency. *Haemophilia* 14: 1255–60

Morishima Y, Tanabe K, Terada Y, Hara T, Kunitada S (1997) Antithrombotic and hemorrhagic effects of DX-9065a, a direct and selective factor Xa inhibitor: comparison with a direct thrombin inhibitor and antithombin III-dependent anticoagulants. *Thromb Haemost* 78:1366–71

Nicholas SB, Aguiniga E, Ren Y, Kim J, Wong J, Govindarajan N, Noda M, Wang W, Kawano Y, Collins A, Hsueh WA (2005) Plasminogen activator inhibitor-1 deficiency retards diabetic nephropathy. *Kidney Int* 67:1297–307

Nighoghossian N, Hermier M, Adeleine P, Blanc-Lasserre K, Derex L, Honnorat J, Philippeau F, Dugor JF, Froment JC, Trouillas P (2002) Old microbleeds are a potential risk factor for cerebral bleeding after ischemic stroke: a gradient–echo T2*-weighted brain MRI study. *Stroke* 33:735–42

Stroke Therapy Academic Industry Roundtable (STAIR) (1999) Recommendations for standards regarding preclinical neuroprotective and restorative drug development. *Stroke* 30:2752–8

The National Institute of Neurological Disorders and Stroke rt-PA Stroke Study Group (1995) Tissue plasminogen activator for acute ischemic stroke. *N Engl J Med* 333:1581–7

The National Institute of Neurological Disorders and Stroke rt-PA Stroke Study Group (1997) Intracerebral hemorrhage after intravenous t-PA therapy for ischemic stroke. The NINDS t-PA Stroke Study Group. *Stroke* 28:2109–18

Umemura K, Wada K, Uematsu T, Nakashima M (1993) Evaluation of the combination of a tissue-type plasminogen activator, SUN9216, and a thromboxane A2 receptor antagonist, vapiprost, in a rat middle cerebral artery thrombosis model. *Stroke* 24: 1077–1082

Vaughan DE, De Taeye BM, Eren M (2007) PAI-1 antagonists: predictable indications and unconventional applications. *Curr Drug Targets* 8:962–70

Weisberg AD, Albornoz F, Griffin JP, Crandall DL, Elokdah H, Fogo AB, Vaughan DE, Brown NJ (2005) Pharmacological inhibition and genetic deficiency of plasminogen activator inhibitor-1 attenuates angiotensin II/salt-induced aortic remodeling. *Arterioscler Thromb Vasc Biol* 25:365–71

Wong KS, Chan YL, Liu JY, Gao S, Lam WW (2003) Asymptomatic microbleeds as a risk factor for aspirin-associated intracerebral hemorrhages. *Neurology* 60:511–3

///// Cutting Edge /////

擬似分子プローブと標的分子構造に基づく *de novo* 医薬分子設計法の開発

東田欣也[1]、後藤純一[1]、平山令明[2]
1. 株式会社菱化システム科学技術システム事業部計算科学部
2. 東海大学医学部

1. はじめに

医薬分子の *de novo* デザイン手法の一つに、標的分子（多くの場合はタンパク質）との結合に深く関与する原子団（以下反応原子団）を含む部分化学構造をつなぎ合わせて新規仮想分子を構築する方法がある。しかし、部分化学構造とそれらを連結する化学構造（リンカー）を機械的に組み合わせると、膨大な仮想分子が発生してしまう。そこで、標的分子の構造情報を最大限に活用し、かつ標的分子への親和性の高い仮想分子を発生させる強力なアルゴリズムが必要になる。このようなコンセプトで作られたアルゴリズムが現在ない訳ではないが、その殆どが実用性という観点から必ずしも満足のいくものではなく、より強力なアルゴリズムの開発が望まれてきた。

さて、X線解析等で得られた標的分子の結合部位情報に基づいて、その部位に結合できる新規の分子をデザインする場合、まず決定すべきことは、結合部位内に配置すべき反応原子団の位置である。この作業が*de novo*デザインにおいて、最も重要であり、かつ最も難しいステップでもある。我々は、この作業を合理的かつ能率的に遂行するために、擬似分子プローブという新しいコンセプトを用いた*de novo*医薬分子デザインのアルゴリズムであるPseudo Molecular Probe (PMP) 法を開発した[1]。

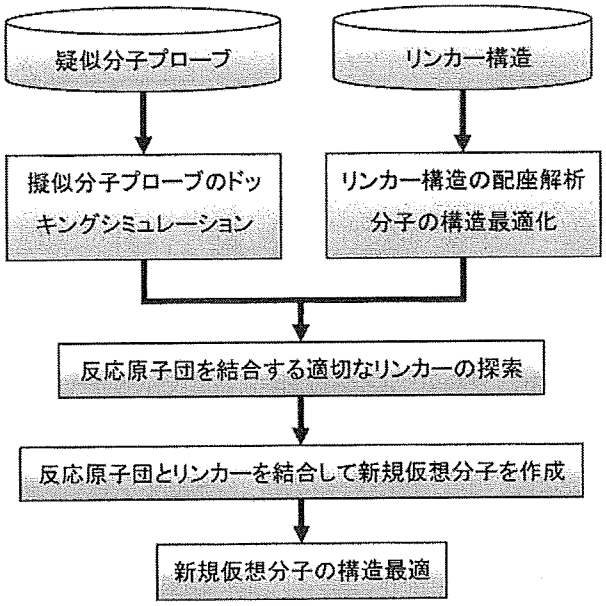

図1　PMP法のフローチャート